

# PETROLOGICAL AND GEOCHEMICAL CHARACTERISATION OF A PORPHYRITIC FELSIC ROCK FROM THE NORTH-EASTERN PART OF CGGC,INDIA



*Thesis submitted for partial fulfillment of M.Sc. Degree  
in Applied Geology, 2018-2019*

SAYANTAN CHAKRABORTY  
ROLL NO: MGEO194020  
DEPARTMENT OF  
GEOLOGICAL SCIENCES

**PETROLOGICAL AND GEOCHEMICAL  
CHARACTERIZATION OF A PORPHYRITIC  
FELSIC ROCK FROM THE NORTH EASTERN  
PART OF  
CHOTONAGPUR GRANITE GNEISS COMPLEX**

*Thesis submitted for partial fulfillment of M.Sc.Degree in  
Applied Geology for the year 2019-2020*

**SAYANTAN CHAKRABORTY**

**ROLL NO: MGEO194020**

**DEPARTMENT OF GEOLOGICAL SCIENCES**

**JADAVPUR UNIVERSITY**

*Under the guidance of*

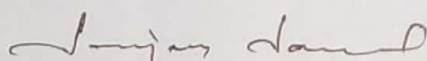
**Prof. Sanjoy Sanyal**



**CERTIFICATE FROM THE SUPERVISOR**

This is to certify that **Mr. Sayantan Chakraborty** has worked under the supervision of Prof. Sanjoy Sanyal in the Department of Geological Sciences, Jadavpur University and completed his thesis entitled **"Petrological and Geochemical Characterization of a Porphyritic Felsic rock, from the north eastern part of CGGC, India"** which is being submitted towards the partial fulfillment of his M.Sc. Final Examination in Applied Geology of Jadavpur University in 2019.

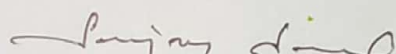
Signature of the Supervisor:

  
30-05-2019

Prof. Sanjoy Sanyal  
Dept. of Geological Sciences  
Jadavpur University

**Dr. Sanjoy Sanyal**  
Professor  
Department of Geological Sciences  
Jadavpur University  
Kolkata: 700032, India

Signature of Head of the Department:

  
30-05-2019

Prof. Sanjoy Sanyal  
Dept. of Geological Sciences  
Jadavpur University

Head  
Department of Geological Sciences  
Jadavpur University  
Kolkata-700032

# CONTENTS

---

<b>Chapter 1: Abstract</b> .....	1-2
<b>Chapter 2: Introduction</b> .....	3
<b>Chapter 3: Regional Geology</b> .....	4-8
<b>Chapter 4: Lithology</b> .....	9-14
<b>Chapter 5: Petrography</b> .....	15-17
<b>Chapter 6: Mineral Chemistry</b> .....	18-26
<b>Chapter 7: Zircon Saturation Temperature</b> .....	25-27
<b>Chapter 8: Geochemistry</b> .....	28-36
<b>Chapter 9: Discussion</b> .....	37-44
<b>Chapter 10: Mineral Abbreviations</b> .....	45
<b>Chapter 11: References</b> .....	46-48
<b>Chapter 12 :Acknowledgement</b> .....	49

# ABSTRACT

The porphyritic felsic rock, exposed near Massanjore in Dumka district, Jharkhand, has been studied with an aim to decipher the geochemical characteristics of the pristine magma. The rock is deformed and metamorphosed and occasionally holds enclaves of mafic granulites and migmatitic felsic gneiss. At places, deformed mafic dykes (now amphibolite) also intruded the porphyritic felsic gneiss. The Porphyritic Felsic Gneiss, has been characterised in the field as a Felsic Augen Gneiss from outcrop view. It majorly contains Alkali Feldspar (Kfs), Plagioclase (Pl), Quartz (Qtz), Orthopyroxene (Opx), Clinopyroxene (Cpx), Garnet (Grt) and Amphibole (Amp) as the major constituents, with presence of some other accessory phases like Zircon and Apatite. Under the microscope, the most notable reaction texture that is observed is between Cpx and Pl, leading to the formation of Grt and Qtz. Upon geochemical analysis, it was determined that the rock belonged to Granodiorite composition, highly ferroan, mostly calc alkaline to slightly calcic and majorly metaluminous to slightly peraluminous in character. The Primitive mantle normalised trace element spider diagram showed a monotonously decreasing abundance pattern, from the most incompatible side to less incompatible side, with depletion of Cs, Ti and Sr and moderate enrichment of Rb, Ba and Ta. The Chondrite normalised REE plot shows a slightly negative slope, with flat HREE trends and moderately enriched LREE trends, with a moderately negative Eu-anomaly. The melt was more Na<sub>2</sub>O rich than K<sub>2</sub>O, which might indicate to the presence of Amp at the source, during melting, but high Ga/Al ratio, high Rb and Ba contents indicate Biotite melting at the

source. The high HFSE contents, with high  $Ta_N$  and  $Nb_N$  data indicates a clear involvement of mantle input with the major continental crust, during the formation of the Porphyritic granitoid. From the plots of Whalen et al(1987) , the rock is classified as an A type granitoid , which was further classified as an  $A_2$  type granitoid by the plots of Eby et al(1990,1992), which characterises it to have formed in a post orogenic setup. In the plots of Pearce et al (1984), the tectonic affinity of the granitoid was classified as a “WPG” or within plate granite. The temperature of the magma was calculated from Zircon saturation, by the formulae of Watson et al(1983) and Boehnke et al(2007) and was found to be  $820\pm 26^\circ\text{C}$  (Watson et al) and  $773\pm 29^\circ\text{C}$  (Boehnke et al) respectively.

## INTRODUCTION

The CGGC is characterized by a granite gneissic complex basically, consisting of a range of rock types, from granulites to even quaternary sediments of Indo-Gangetic plain. My studied area, Massanjore, is characterized by the presence of both mafic and felsic rocks, characterized by the presence of both garnetiferous, as well as garnet absent amphibolites, mafic granulites, porphyritic charnockites, migmatitic felsic gneiss and leucogranites. My study encompasses only the porphyritic charnockites, also known as the porphyritic augen gneiss

- Objectives of study :

I have restricted myself to the petrological and geochemical study of the porphyritic charnockite and have tried to establish the following :

- The nature of magma source
- The origin of the melt
- The tectonic affinity
- Temp of the melting

## Regional geology of **CGGC**:

The Chotanagpur Granite Gneissic Complex( CGGC ) forms an important part of the East Indian Shield, along with the Archaean Singhbhum Craton, which is separated from the CGGC by the Palaeoproterozoic, North Singhbhum Fold Belt, which trends E-W to NW-SE. The CGGC is recognized as a mobile belt, belonging to the part of Central Indian Tectonic Zone(CITZ), an E-W–trending regional suture, through which major Indian blocks got stitched together in Palaeo-Neoproterozoic time (e.g. Acharyya, 2003; Bhowmik et al.,2012). However, the omnipresence of Phanerozoic sediment cover, in the western part of the CGGC, prevents further detailed correlations between the CGGC and the Central Indian Tectonic Zone. Gangetic alluvium spreads over the northern part of CGGC, whereas the eastern margin of the terrain is covered by Phanerozoic sediments of Bengal Basin and Rajmahal Trap volcanics.

Previously published geological and geochronological data, by Sanyal and Sengupta (2012), reveals that porphyritic granitoids and charnockites ( pyroxene-bearing granitoids ), together termed as “felsic orthogneiss”. This comprises the major country-rock of the terrain, with several enclaves of different rock types, that vary in lithology, from mafic granulites, khondalites (i.e., garnet-sillimanite gneiss), calc-silicates , even to minor quartzite. A large body of a massif-type anorthosite, better known as the Bengal Anorthosite, is located in the southeastern part of the terrain (Chatterjee et al., 2008). Several alkaline bodies have intruded the felsic orthogneisses in the southern part of the terrain, near the North Puruliya Shear Zone (NPSZ) and the South Purulia Shear Zone(SPSZ).

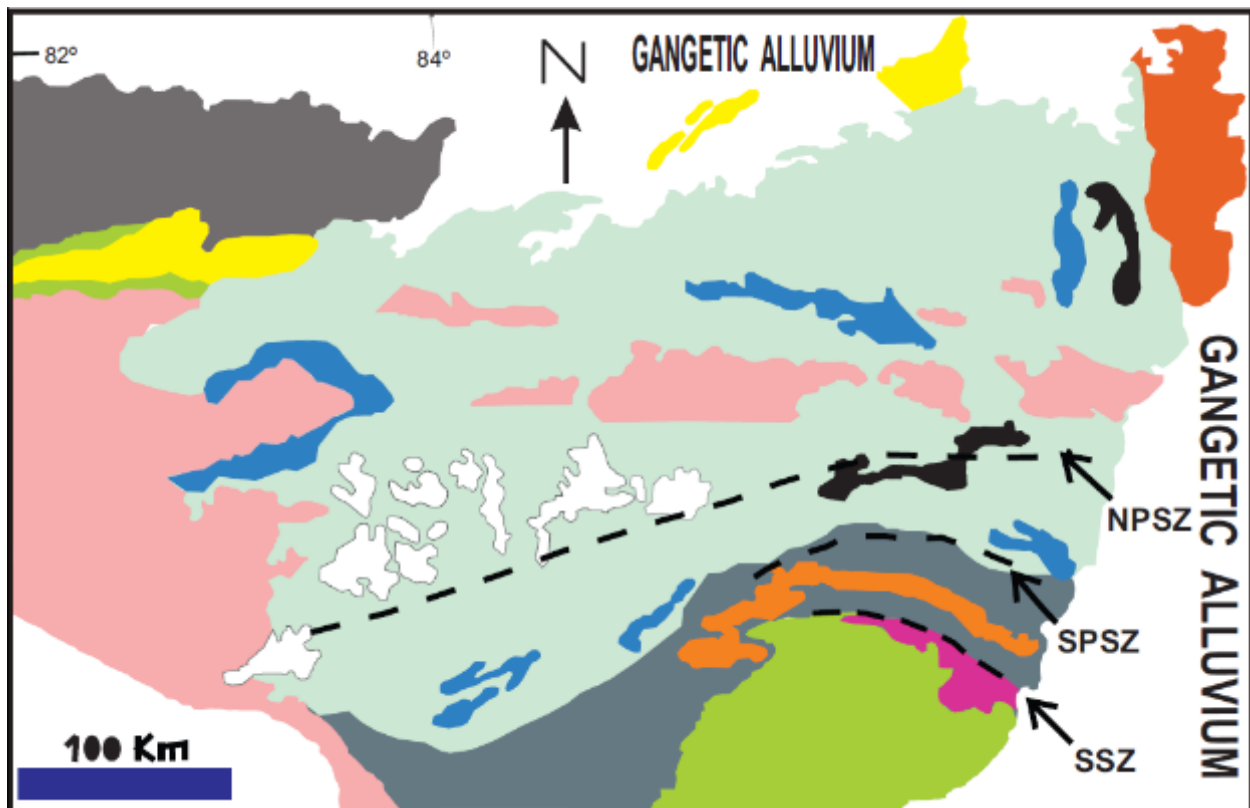
Indications of the presence of three major phases of deformation & metamorphism (MI, MII, MIII), experienced by the CGGC, can be ascertained from the geochronological and petrological data published till date (Chatterjee et al., 2010; Ghosh and Sengupta, 1999; Maji et al., 2008; Mukherjee et al., 2017; Sanyal and Sengupta, 2012). Meta-pelitic enclaves record the oldest metamorphic event represented by an ultra-high temperature metamorphism (UHT) at moderate pressure (8 kbar) (Sanyal and Sengupta, 2012), which culminated at  $\sim 1650$  Ma (Dey et al., 2017). The porphyritic granite intruded into the northern and western part of the terrain within 1750 Ma and 1660 Ma (Chatterjee and Ghose, 2011; Saikia et al., 2017). U-Pb zircon data estimate an age of  $1550 \pm 12$  Ma as the emplacement age of the massif anorthosite in the south-eastern part (Chatterjee et al., 2008). Magmatism in the eastern part of the terrain extended further into the Mesoproterozoic, as revealed by the intrusion of syenite body near Dumka, that yielded a Rb-Sr age of  $1475 \pm 63$  Ma (Ray Barman and Bishui, 1994).

The most pervasive metamorphic event, affecting the CGGC, as evident from different lithological units, occurred under high-pressure upper-amphibolite to granulite-grade conditions with peak P-T of around 750–800 °C and 9–11 kbar, reflecting a phase of continent–continent collision that took place around 1200–950 Ma (Chatterjee and Ghose, 2011; Karmakar et al., 2011; Maji et al., 2008; Mukherjee et al., 2017; Rekha et al., 2011). Subsequent intrusion of mafic dykes was followed by an amphibolite grade metamorphic event (600–750 °C at  $7 \pm 1$  kbar; Sanyal and Sengupta, 2012) that occurred between 870–780 Ma (Chatterjee et al., 2010; Sanyal and Sengupta, 2012). However, Chatterjee et al. (2010) inferred this event as a high-grade

metamorphism reaching a pressure of  $\sim 12$  kbar at  $730^{\circ}\text{C}$  associated with the Eastern Indian Tectonic Zone (EITZ). Detailed geochemical data of the granitoids are scarce from the vast terrain and only reported by few workers (Goswami and Bhattacharyya, 2013; Lalnunmawia et al., 2011; Saikia et al., 2017; Singh and Krishna, 2009; Yadav et al., 2014).

Porphyritic granites near Gaya are characterized as A-type granites formed by the high-temperature melting of lower to middle crust with varying mantle input (Yadav et al., 2014) and has intruded at 1697 Ma (Chatterjee and Ghose, 2011). On the contrary, granites in the north-western part are inferred to be arc-related magma, which intruded between 1750–1660 Ma (Saikia et al., 2017).

My study area is Massanjore, which is located in the north eastern part of CGGC, at the southern tip of Dumka District, in Jharkhand.



### INDEX

	<b>A</b>		<b>D</b>		<b>G</b>		<b>J</b>
	<b>B</b>		<b>E</b>		<b>H</b>		<b>K</b>
	<b>C</b>		<b>F</b>		<b>I</b>		

- A- Vindhyan Supergroup of rocks
- B- Metasediments in CGGC
- C- Gondwana rocks
- D- Quarternary sediments
- E- Rajmahal Basalt
- F- Granulite Domains
- G- CGGC Gneissic rocks
- H- Dalma Volcanics
- I- Singbhum and other Granites
- J- SMB Metamorphics
- K- Mahakoshal Group of rocks

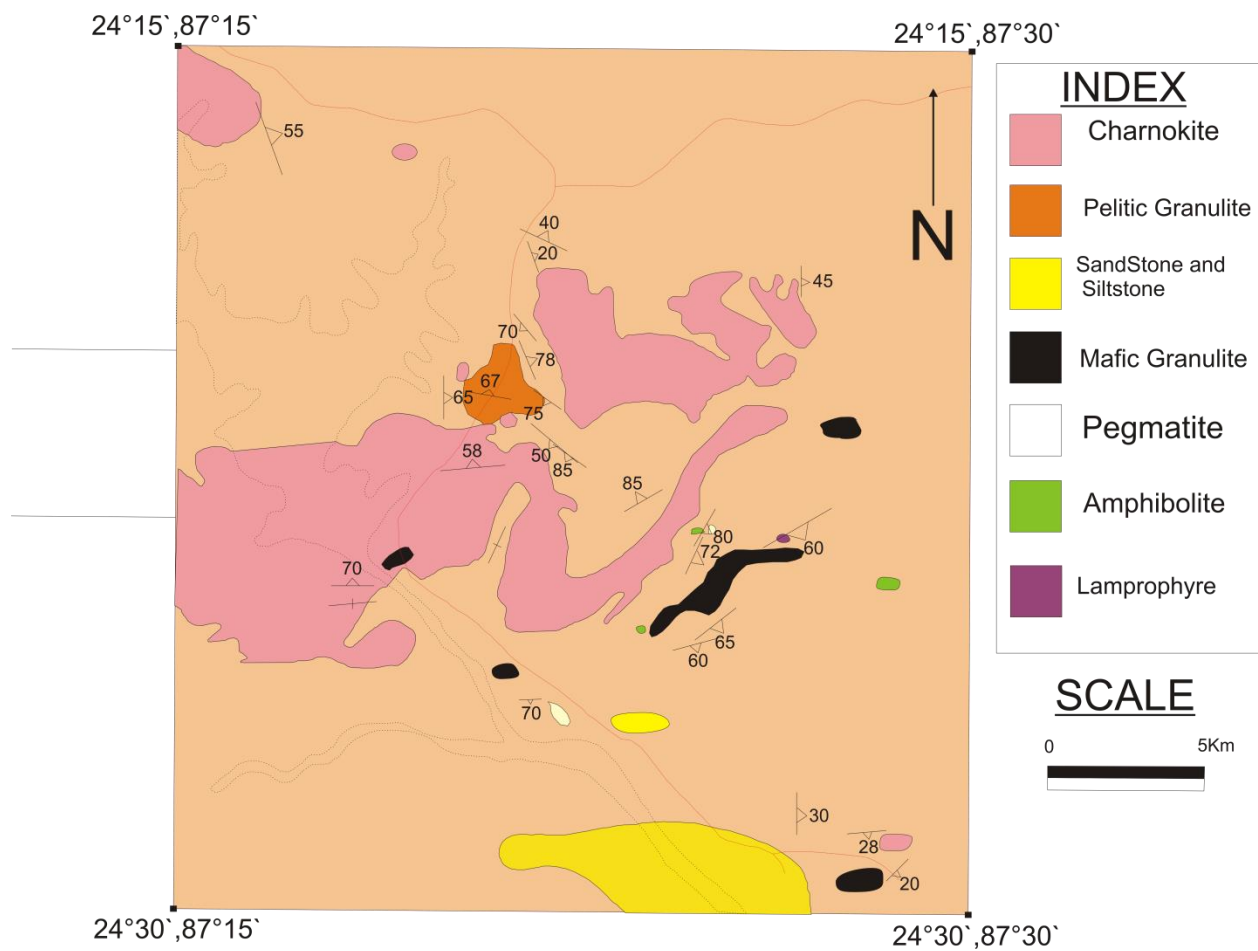


Fig. The Representative geological map of the study area

## **LITHOLOGY**

The study area, Masanjore is situated at the eastern margin of CGGC in the district of Dumka, Jharkhand. The rock units in these areas are spatially distributed covering Ranishawr-Sadipur-Murjora-Ranibahal area, Dam area, Bagnal and extending upto Patabari and Ragnali-Asanbani area. The major rock type in and around Massanjore, Jharkhand broadly is felsic in nature. It mainly consists of three types of felsic units. These felsic units include an augen gneiss or porphyritic granite, a migmatitic gneiss and a leucogranite. Apart from these felsic units which form the country rock of the area other metapelitic bodies and mafic units are present within the country rock as enclaves or intrusive bodies. Studying the different rock types and the structures shown by them help to understand the deformation history of the area and its relationship with the evolution of the Chotanagpur Gneissic Complex.

Coming to the descriptive part of the different felsic units observed and studied in and around Massanjore area, we have to deal with three rock units. The most abundant and major rock unit forming the country rock of the area is the migmatitic felsic gneiss. Though overall the rock is medium to fine grained, it is highly banded and these leucosomal bands consisting of quartz and feldspars are comparatively coarser than the host rock unit(Fig 1c). Beads of garnets are present within this leucosomal banding along with its host. But again, garnets are coarser and more abundant in the leucosomal part.. This rock is a partially melted migmatitic gneiss and shows upto third generation of folding(Fig 1d). The trend and plunge of fold axis  $F_2$  :  $37^\circ \rightarrow 110^\circ$ . The rock unit shows thickened hinge areas and pinch and swell structures in the limb part. Clinopyroxene is present in the rock unit. Sometimes this rock type showed thinly banded nature and an overall charno-

enderbitic composition. The general trend of  $F_3$  fold axis is  $155^\circ$ . Laterally continuous bands associated with  $S_2$  are seen and this entire unit is intruded by a mafic dyke.  $F_1$  and  $F_2$  folds are coaxial.

The rock shows a spotted nature, consisting of large potash feldspar grains, jacketed with quartz and garnet (Fig 1a). The rock shows a bluish gray colour, and a greasy appearance, typical of a charno-enderbitic rock. The feldspar grains are quite large in size (even up to 4cm-5cm) and show typical butterfly twinning indicating its igneous origin. Garnet appears as a chain like structure around the stretched feldspar porphyroclasts. Amphibole crystals, also form a jacket around the feldspar grains and are also distributed throughout the rock. Enclaves of the felsic country rock present within this rock body implies its later intrusion compared to the other. The bluish grey colour is mainly due to the presence of blue quartz in the rock. The rock shows clear evidences of deformation. The large feldspar grains are stretched along with their halo (Fig 1b) and gives an eye shaped appearance, which compels us to acknowledge them as feldspar augens. The stretching of feldspar grains only indicate a high temp metamorphic event. So, the once emplaced porphyritic granite was metamorphosed to form Augen Gneiss. In several exposures, the augen gneiss shows to have enclaves of mafic rock and the migmatitic felsic gneiss. The  $S_1$  plane of the feldspar augen gneiss coincides with the  $S_2$ .

The last major felsic rock type is a leucogranite (Fig 1e). This rock is highly deformed and contains elongated grains of biotite on the foliation plane giving it a streaky appearance (Fig 1f), also called as streaky gneiss with two prominent layers of fine and coarse grains. All these three rock units are later intruded by a coarse-grained pegmatitic unit.

The mafic granulite body is present within this felsic country rocks. Amphibole, pyroxene, garnet and plagioclase are the major constituents of this mafic rock. Due to the variation in grain size this rock can be divided into two types. The first type encountered is a host mafic granulite medium to fine-grained with various other features( Fig 2b). The rock is well-foliated with a general trend of  $220^{\circ}$  and containing good amount of garnet grains. The foliation is defined by the amphibole grains. These garnet grains occur as clusters are small in size. The rock is very hard in nature Patches of melts are also present within the host rock type. The next type is a similar to the first type with very large pinkish red garnet grains spread throughout the rock unit(Fig 2c), also called as measles garnet. Around the garnet grain a halo of amphibole and plagioclase is formed. Feldspathic veins are present within the rock body(Fig 2d). Some feldspathic veins are coarse grained and contains amphibole and profuse garnets. The feldspathic veins are jacketed by amphibole and pyroxene grains.(Fig 2e) These veins are quite thick (5 to 6 cm). apart from this some thin feldspathic veins are present which are not garnetiferous.

Another mafic rock type is that of an amphibolite with felsic veins in some areas(Fig 2a). The rock is medium to fine-grained. In some places this deformed basic rock contains veins of pyroxene. The pyroxene veins are sometimes folded and the foliations of the host basic rock cut the hinge parts of these small scale folds. The general foliation trend is  $185^{\circ}$ .

Two major pelitic rock bodies are also present. One of them shows evidence of profuse melting and forms leucosomal bands which contains large clusteters of garnets. These leucosomal bands are medium to

coarse grained parts of quartz and K-feldspar. Needles of silimanite are also present.

The other pelitic body lacks this kind of leucosomal bands and overall more fine grained and more homogenous than the former one. Along with garnet, cordierite is also present within this rock and gives it a deep blue tinge.

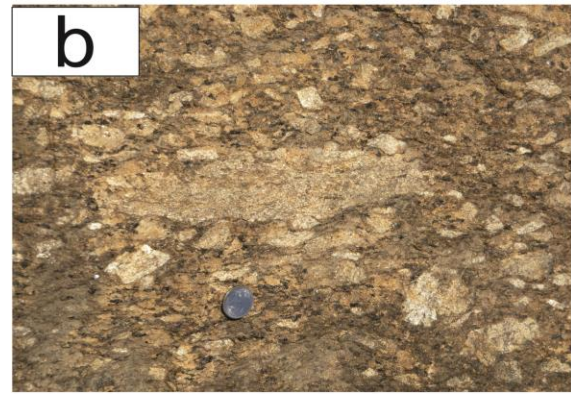
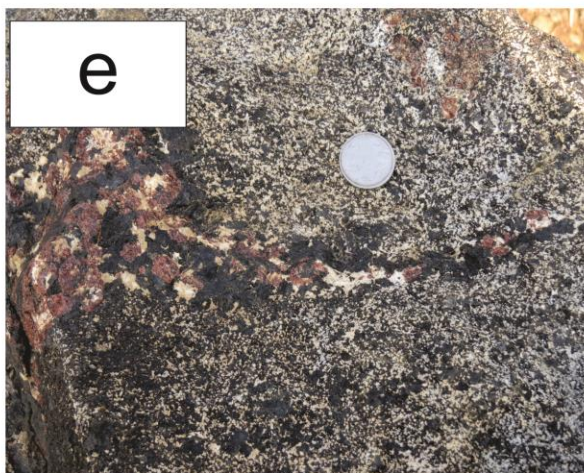
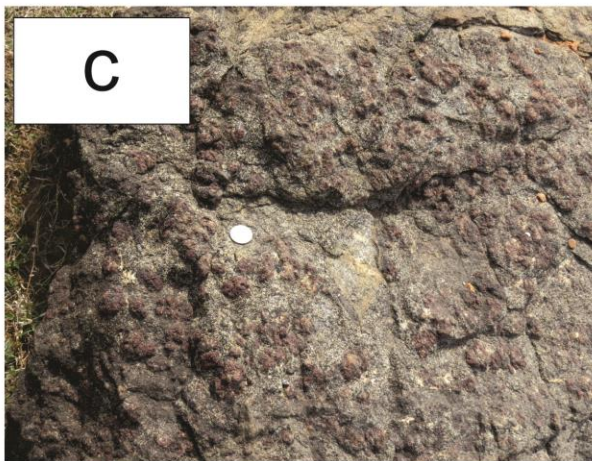
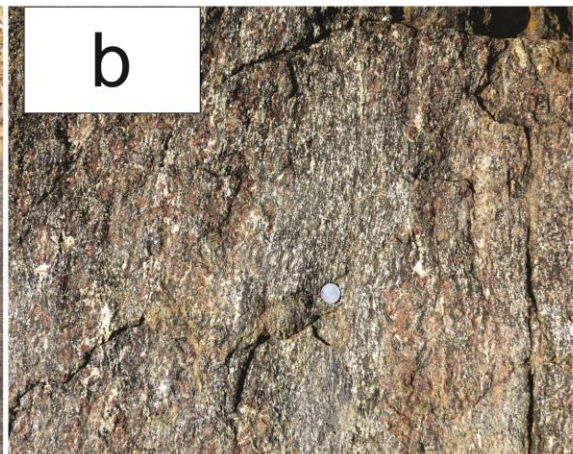


Fig 1(a) and (b) Porphyritic granite or augen gneiss (a) Spotted outcrop of porphyritic felsic gneiss (b) Stretched feldspar grains  
 fig 1 (c) and 1(d) Migmatitic Felsic Gneiss (c) Extremely banded nature (d) Distinct melanosomal and leucosomal bands.  
 Fig 1(e) and 1(f) Leucogranite or streaky gneiss (f) Streaky nature generated by oriented grains of biotite on the foliation plane.



**Fig 2(a)** Amphibolite with thread like felsic veins.

**2(b)** Mafic granulite with clusters of small Garnet grains.

**2( c)** Mafic granulite with clusters of large garnets , measles like appearance.

**2(d)** Feldspathic veins with wall controlled garnet growth .

**2(e)** Feldspathic veins, within mafic granulites, jacketed with pyroxene and amphibole

## Petrography :

The rock is dominated by feldspar, mostly alkali feldspar, then plagioclase and microcline. It also contains quartz in considerable amounts. Both quartz and Feldspar grains show bimodal occurrence (Fig 3a), where some of the Feldspar grains are porphyritic in nature and others are found in the groundmass. Cpx, Opx, Hbl, opaques and Grt are also found. Opaques also show bimodal occurrence (Fig 3f), where some are larger, subhedral to mostly anhedral in nature and some are quite small, even speck like. Opaques are associated with hornblende and Cpx. Two different types of opaques are present, viz. Ilmenite and Magnetite. There are two types of hornblende grains, some are cloudy and seen to be replacing the Cpx grains, whereas the others are euhedral and quite clear in appearance. The Grt grains are mostly small and rounded, bead like in nature. They are connected in such a way, that it gives a chain like appearance. In most of the cases, Grt grains show inclusions of Quartz. There is also a presence of high relief mineral, showing variegated green–pink interference colour, called Sphene, though sometimes they are also observed to be mimicking their body colour under XPL. There is also presence of good amounts of Myrmakite (Fig 3e).

The most distinct reaction that is observed, is a reaction texture involving Cpx, Plag, Grt, Qtz. As the texture suggests, it is a rxn between Cpx and Plag, leading to the formation of Grt and Qtz.



This reaction works as an excellent barometer, where Grt and Qtz assemblage indicates a higher pressure assemblage. Most of the

grains show clear evidences of deformation. Deformation is reflected by the suturing of Qtz grains, deformed lamellar twins, for plagioclase, deformed cross hatched twinning, in case of microcline. In some cases, proper dihedral angles are also observed, between Qtz and Feldspar grains, exhibiting an equilibrium texture.

At a later stage, the Feldspar grains show extensive alteration, sometimes saussuritised and sometimes sericitized. In some cases, Cpx and Opx both seem to have been altered to form Hbl.

So, essentially, the rock is of a composition of an Opx bearing Granite and local pockets of melting as observed from the samples, indicate a high temperature metamorphic event , maybe even of granulite facies and thus , the rock can be named as a charnokite and because of the presence of alkali feldspar phenocrysts , it can be called as a porphyritic charnokite.

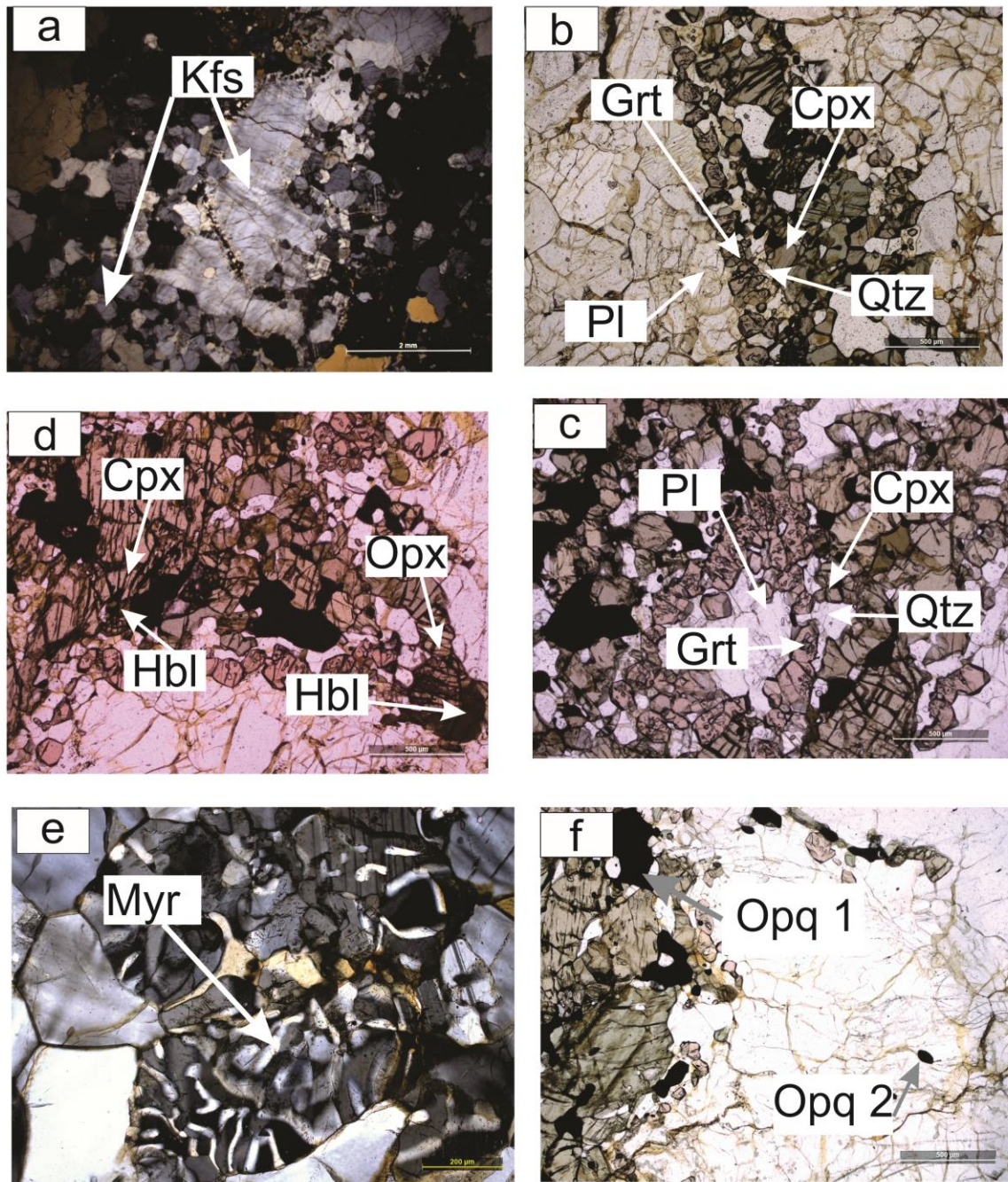


**Fig 3**(a)Photomicrograph showing Kfs phenocrysts and bimodal distribution of Kfs  
**(b) and (c)** Photomicrograph showing reaction texture between Cpx and Pl ,  
 leading to the formation of Grt and Qtz.**(d)** Opx and Cpx get altered to form Hbl.  
**(e)** Extensive myrmakite formation throughout the rocks.  
**(f)** Bimodal distributio of Opaque minerals

## **MINERAL CHEMISTRY**

### *Analytical Technique*

Chemical composition of the minerals are determined from carbon-coated thin section of rocks by electron microprobe analysis with CAMECA Sx100 Electron Probe Micro Analyzer at the EPMA, Laboratory, Central Petrological Laboratory, Geological Survey of India, Kolkata. At the Central Petrological Laboratory, Geological Survey of India, Kolkata, the accelerating voltage was 15KV with 12nA current conditions. The beam diameter was 1 micron. Natural mineral standard except for Mn and Ti for which synthetic standard were used and the raw data were corrected by PAP procedure (Pouchou and Pichoir, 1984).

**Representative mineral compositions are presented in table ... The salient compositional features are represented below:**

#### **Orthopyroxene :**

The orthopyroxene is highly ferroan in character, with  $X_{Fe}$  ranging from 0.681-0.649; core to rim, which is not a major variation, but this variation shows a significant drop, mostly at the opx-cpx boundaries and a consequent spike in  $X_{Mg}$ . Alumina content also decreases from 0.51 wt% at the core to 0.41wt% at the rim. CaO content also decreases from 0.69wt% at the core to 0.41wt% at the rim.

**Clinoproxene :**

The clinopyroxene is and  $X_{Mg}$  increases from 0.438 at the core to 0.449 at the rim, near the plagioclase cpx boundary, where as  $X_{Fe}$  decreases from 0.561 at the core to 0.55 at the rim of plagioclase and cpx boundary. Alumina content is much much higher at around 1.19wt% - 1.38wt%, as compared to Opx.

**Garnet :**

Garnet belongs to pyrope series and is dominated by almandine and grossular components with minor pyrope and spessartine components respectively. The garnet grains do not show any characteristic variation in  $X_{Alm}$  along core to rim, ranging between 0.68-0.66. Also, there is no distinct variation in case of  $X_{Grs}$ , ranging from 0.22 to 0.19,  $X_{Pyr}$ , ranging from 0.08-0.05 and  $X_{Spss}$ , ranging from 0.04-0.03.

**Ilmenite :**

Ilmenite does not show much variation in terms of  $X_{Fe}$  or  $X_{Ti}$ , except for ilmenite inside Garnet grains, which show a decrease in Ti content (around 0.487), from an average concentration (around 0.5).  $Fe_2O_3$  content is also zero in most cases, except for those grains inside the garnet, which shows a minor amount of  $Fe_2O_3$  (around 0.322)

**Biotite :**

Biotite is mostly ferroan in nature, with  $X_{Fe}$  ranging from 0.62- 0.63, but for biotite grains included within garnet,  $X_{Fe}$  shows a stark decrease to around 0.55.  $TiO_2$  varies from 5.56wt%-5.92wt%.

**Amphibole :**

According to the classification scheme of Leake et al. (1997) amphiboles are dominantly calcic in nature and are enriched in Fe as well. They generally are ferropargasite in nature.  $X_{Mg}$  varies from 0.31 to 0.36, where as  $X_{Fe}$  ranges from 0.69 to 0.64. It is interesting to note that the Amphiboles in Garnet, shows higher  $X_{Mg}$  (around 0.34) and thus lower  $X_{Fe}$  (around 0.66) than other amphiboles.  $TiO_2$  content also varies from 1.94% to 2.26% in case of matrix grains, but in case of amphiboles in garnet, shows a bit higher value of  $TiO_2$  (around 2.33%).

**Plagioclase :**

Plagioclase is mostly albitic in nature,  $X_{Ab}$  ranging from 0.69 to 0.65 and  $X_{An}$  ranging from 0.35 to 0.29, with some minor  $X_{Orth}$  components of around 0.01.

**Orthoclase :**

The K-Feldspar grains are highly potassic in character, with K-Feldspar component is of 92%.

**Magnetite :**

The magnetite is mostly Fe III dominated and Fe III : Fe II ratio is around 1.94.

Table Number 3. Mineral Chemistry of different mineral phases

DataSet/Point	66 / 1 .	67 / 1 .	84 / 1 .	28 / 1 .	33 / 1 .	73 / 1 .	74 / 1 .
Phase	Opx-r	Opx-c	Opx-c	Opx	Opx-r	Cpx^PI	Cpx-c
Al <sub>2</sub> O <sub>3</sub>	0.41	0.51	0.54	0.56	0.39	1.19	1.27
FeO	37.88	38.14	37.81	36.15	37.91	17.48	17.86
TiO <sub>2</sub>	0.05	0.08	0.05	0.08	0.03	0.14	0.15
ZnO	0.00	0.00	0.00	0.00	0.00	0.00	0.00
SiO <sub>2</sub>	49.22	49.11	49.12	49.21	49.86	51.10	49.97
K <sub>2</sub> O	0.02	0.02	0.01	0.00	0.00	0.01	0.01
CaO	0.53	0.69	0.69	0.62	0.41	21.38	21.03
Na <sub>2</sub> O	0.00	0.00	0.07	0.00	0.00	0.40	0.43
Cr <sub>2</sub> O <sub>3</sub>	0.02	0.03	0.00	0.00	0.00	0.00	0.00
MnO	0.65	0.65	0.62	0.49	0.58	0.27	0.30
MgO	10.23	10.21	9.91	10.95	11.09	8.02	7.81
NiO	0.00	0.00	0.00	0.00	0.00	0.00	0.00
GT	99.01	99.44	98.82	98.06	100.27	99.99	98.83
Al	0.024	0.029	0.031	0.027	0.019	0.062	0.067
FeIII	0.000	0.000	0.000	0.000	0.000	0.000	0.000
Fe	<b>1.545</b>	1.548	1.537	1.245	1.281	<b>0.643</b>	0.665
Ti	<b>0.002</b>	0.003	0.002	0.002	0.001	<b>0.005</b>	0.005
Zn	0.000	0.000	0.000	0.000	0.000	0.000	0.000
Si	2.401	<b>2.383</b>	<b>2.387</b>	2.026	2.014	2.248	<b>2.223</b>
K	0.001	<b>0.001</b>	<b>0.001</b>	0.000	0.000	0.001	<b>0.001</b>
Ca	0.028	0.036	0.036	0.027	0.018	1.008	1.003
Na	0.000	0.000	0.007	0.000	0.000	0.034	0.037
Cr	0.001	0.001	0.000	0.000	0.000	0.000	0.000
Mn	0.027	0.027	0.026	0.017	0.020	0.010	0.011
Mg	0.744	0.738	0.718	0.672	0.668	0.526	0.518
Ni	0.000	0.000	0.000	0.000	0.000	0.000	0.000
Soma-Cát.	4.771	4.766	4.743	4.017	4.020	4.536	4.529
Soma-O	7.185	7.167	7.144	6.059	6.044	6.802	6.772
X <sub>Fe</sub>	0.675069095	0.676996	0.6816	0.649409	0.657298	0.449863	0.438005

DataSet/Point	62 / 1 .	76 / 1 .	63 / 1 .	46 / 1 .	47 / 1 .	56 / 1 .	69 / 1 .
Phase	Gt-r	Gt-c	Gt-c	Gt-c	Gt- r^Amph	Gt-r	Kfs in Aper
Al <sub>2</sub> O <sub>3</sub>	20.52	20.29	20.52	20.51	19.51	20.28	18.27
FeO	28.98	30.91	30.68	30.89	31.24	30.74	0.00
TiO <sub>2</sub>	0.02	0.03	0.00	0.03	0.06	0.00	0.00
ZnO	0.00	0.00	0.00	0.00	0.00	0.00	0.00
SiO <sub>2</sub>	37.92	37.65	37.60	37.61	37.34	37.11	64.64
K <sub>2</sub> O	0.00	0.00	0.03	0.00	0.00	0.00	15.86
CaO	7.77	7.38	7.38	6.89	7.19	7.75	0.03
Na <sub>2</sub> O	0.01	0.01	0.01	0.00	0.00	0.06	0.80
Cr <sub>2</sub> O <sub>3</sub>	0.00	0.12	0.00	0.00	0.04	0.02	0.00
MnO	1.83	1.95	1.84	1.48	1.6	1.5	0.00
MgO	1.73	1.63	1.77	2.06	1.94	1.64	0.00
NiO	0.00	0.00	0.00	0.00	0.00	0.00	0.00
GT	98.78	99.97	99.83	99.47	98.92	99.1	99.60
Al	1.958	1.922	1.942	1.947	1.868	1.934	0.999
FeIII	0.000	0.016	0.022	0.000	0.00	0.00	0.000
Fe	1.962	2.061	2.039	2.080	2.066	2.011	0.000
Ti	<b>0.001</b>	0.002	0.000	0.002	0.004	0.000	0.000
Zn	<b>0.000</b>	0.000	0.000	0.000	0.000	0.000	2.998
Si	3.070	3.026	3.020	3.029	3.033	3.003	0.938
K	0.000	<b>0.000</b>	<b>0.003</b>	0.000	0.000	0.000	0.001
Ca	0.674	<b>0.636</b>	<b>0.635</b>	0.594	0.626	0.672	0.072
Na	0.002	0.002	0.002	0.000	0.000	0.009	0.000
Cr	0.000	0.008	0.000	0.000	0.003	0.001	0.000
Mn	0.125	0.133	0.125	0.101	0.110	0.103	0.000
Mg	0.209	0.195	0.212	0.247	0.235	0.198	0.000
Ni	0.000	0.000	0.000	0.000	0.000	0.000	0.000
Soma-Cát.	8.000	8.000	8.000	8.000	8.000	8.000	5.008
Soma-O	12.049	12.000	12.000	12.004	12.000	12.000	8.000
X <sub>Alm</sub>	0.660567374	0.68144	0.6771	0.688163	0.6803446	0.6740953	
X <sub>Gros</sub>	0.226903613	0.210107	0.21094	0.19665	0.2060589	0.2251663	

DataSet/Point	68 / 1 .	79 / 1 .	80 / 1 .	30 / 1 .	37 / 1 .	85 / 1 .
Phase	Ilm	Ilm	Ilm in Gt	Ilm	Ilm symp Gt	Cpx-small
Al <sub>2</sub> O <sub>3</sub>	0.01	0.01	0.01	0.030	0.480	1.38
FeO	45.56	46.41	47.21	45.240	44.825	17.74
TiO <sub>2</sub>	50.68	49.95	50.01	52.440	48.730	0.13
ZnO	0.00	0.00	0.00	0.000	0.000	0.00
SiO <sub>2</sub>	0.00	0.09	0.00	0.030	1.050	50.49
K <sub>2</sub> O	0.00	0.01	0.04	0.000	0.000	0.00
CaO	0.00	0.00	0.02	0.000	0.100	21.24
Na <sub>2</sub> O	0.03	0.02	0.00	0.020	0.010	0.41
Cr <sub>2</sub> O <sub>3</sub>	0.00	0.06	0.00	0.000	0.000	0.01
MnO	0.37	0.32	0.42	0.460	0.350	0.38
MgO	0.20	0.33	0.35	0.340	0.440	7.66
NiO	0.00	0.00	0.00	0.000	0.000	0.00
<b>GT</b>	96.85	97.20	98.06	98.560	95.985	99.44
Al	0.000	0.000	0.000	0.001	0.015	0.072
FeIII	0.000	0.000	0.006	0.000	0.027	0.000
Fe	0.999	1.014	1.017	0.972	0.967	0.655
Ti	0.999	0.982	0.975	1.013	0.945	0.004
Zn	<b>0.000</b>	0.000	0.000	0.000	0.000	0.000
Si	<b>0.000</b>	0.002	0.000	0.001	0.027	<b>2.229</b>
K	0.000	0.000	0.001	0.000	0.000	<b>0.000</b>
Ca	0.000	<b>0.000</b>	<b>0.001</b>	0.000	0.003	1.005
Na	0.002	<b>0.001</b>	<b>0.000</b>	0.001	0.000	0.035
Cr	0.000	0.001	0.000	0.000	0.000	0.000
Mn	0.008	0.007	0.009	0.010	0.008	0.014
Mg	0.008	0.013	0.014	0.013	0.017	0.504
Ni	0.000	0.000	0.000	0.000	0.000	0.000
Soma-Cát.	2.016	2.021	2.023	2.010	2.008	4.519
Soma-O	3.015	3.005	3.000	3.023	3.000	6.771

<b>DataSet/Point</b>	<b>78 / 1 .</b>	<b>82 / 1 .</b>	<b>87 / 1 .</b>	<b>92 / 1 .</b>	<b>29 / 1 .</b>
	<b>Amph in</b>				
<b>Phase</b>	<b>Amph</b>	<b>Gt</b>	<b>Amph</b>	<b>Amph</b>	<b>Amph</b>
<b>Al<sub>2</sub>O<sub>3</sub></b>	1.41	1.46	1.21	1.29	10.8
<b>FeO</b>	5.70	6.23	5.82	5.71	21.3
<b>TiO<sub>2</sub></b>	10.70	10.86	10.95	10.60	2
<b>ZnO</b>	40.75	40.71	41.17	40.01	0.00
<b>SiO<sub>2</sub></b>	1.71	1.74	1.72	1.67	41.44
<b>K<sub>2</sub>O</b>	11.44	11.05	11.06	10.85	1.7
<b>CaO</b>	2.14	2.33	2.13	2.02	11.57
<b>Na<sub>2</sub>O</b>	0.00	0.06	0.00	0.00	1.19
<b>Cr<sub>2</sub>O<sub>3</sub></b>	0.17	0.04	0.08	0.15	0.09
<b>MnO</b>	23.44	22.11	23.11	22.34	0.03
<b>MgO</b>	0.00	0.00	0.00	0.00	6.56
<b>GT</b>	97.46	96.59	97.25	94.64	96.68
<b>Si</b>	6.3796	6.3818	6.4139	6.4131	6.4655
<b>Al (IV)</b>	1.6204	1.6182	1.5861	1.5869	1.5345
<b>Ti</b>	0.0000	0.0000	0.0000	0.0000	0.0000
<b>Sum T</b>	<b>8.0000</b>	<b>8.0000</b>	<b>8.0000</b>	<b>8.0000</b>	<b>8.0000</b>
<b>Al (VI)</b>	0.3545	0.3889	0.4251	0.4162	0.4520
<b>Ti</b>	0.2520	0.2747	0.2496	0.2435	0.2347
<b>Cr +3</b>	0.0000	0.0074	0.0000	0.0000	0.0111
<b>Fe +3</b>	0.0984	0.1075	0.1669	0.1366	0.0225
<b>Mg</b>	1.3299	1.4555	1.3513	1.3640	1.5253
<b>Fe +2</b>	2.9652	2.7660	2.8071	2.8397	2.7544
<b>Mn</b>	0.0000	0.0000	0.0000	0.0000	0.0000
<b>Li</b>	0.0000	0.0000	0.0000	0.0000	0.0000
<b>Sum C</b>	<b>5.0000</b>	<b>5.0000</b>	<b>5.0000</b>	<b>5.0000</b>	<b>5.0000</b>
<b>Mg</b>	0.0000	0.0000	0.0000	0.0000	0.0000
<b>Fe +2</b>	0.0054	0.0252	0.0370	0.0185	0.0024
<b>Mn</b>	0.0225	0.0053	0.0106	0.0204	0.0040
<b>Li</b>	0.0000	0.0000	0.0000	0.0000	0.0000
<b>Ca</b>	1.9191	1.8561	1.8463	1.8635	1.9342
<b>Na</b>	0.0530	0.1134	0.1062	0.0977	0.0594
<b>Sum B</b>	<b>2.0000</b>	<b>2.0000</b>	<b>2.0000</b>	<b>2.0000</b>	<b>2.0000</b>
<b>Ca</b>	0.0000	0.0000	0.0000	0.0000	0.0000
<b>Na</b>	0.3750	0.3304	0.2593	0.3032	0.3006
<b>K</b>	0.3415	0.3480	0.3419	0.3415	0.3384
<b>Sum A</b>	<b>0.7166</b>	<b>0.6784</b>	<b>0.6012</b>	<b>0.6448</b>	<b>0.6390</b>
<b>TOTAL</b>	<b>15.7166</b>	<b>15.6784</b>	<b>15.6012</b>	<b>15.6448</b>	<b>15.6390</b>
<b>X<sub>Fe</sub></b>	<b>0.69</b>	<b>0.66</b>	<b>0.68</b>	<b>0.68</b>	<b>0.64</b>

<b>DataSet/Point</b>	<b>64 / 1 .</b>	<b>65 / 1 .</b>	<b>70 / 1 .</b>	<b>71 / 1 .</b>	<b>72 / 1 .</b>	<b>86 / 1 .</b>
<b>Phase</b>	<b>Pl<sup>^</sup>Gt62</b>	<b>Pl-c</b>	<b>Pl in Aper</b>	<b>Pl-r<sup>^</sup>Cpx</b>	<b>Pl-c</b>	<b>Pl<sup>^</sup>Cpx</b>
<b>Al<sub>2</sub>O<sub>3</sub></b>	24.75	24.12	24.68	24.76	24.72	24.52
<b>FeO</b>	0.36	0.82	0.02	0.23	0.18	0.22
<b>TiO<sub>2</sub></b>	0.02	0.01	0.00	0.01	0.00	0.00
<b>ZnO</b>	0.00	0.00	0.00	0.00	0.00	0.00
<b>SiO<sub>2</sub></b>	60.47	60.50	61.91	60.62	60.81	60.64
<b>K<sub>2</sub>O</b>	0.30	0.31	0.20	0.33	0.18	0.25
<b>CaO</b>	6.76	6.64	6.33	6.86	6.92	6.72
<b>Na<sub>2</sub>O</b>	7.69	7.78	8.12	7.81	7.52	7.89
<b>Cr<sub>2</sub>O<sub>3</sub></b>	0.00	0.00	0.00	0.00	0.06	0.00
<b>MnO</b>	0.01	0.05	0.04	0.03	0.00	0.01
<b>MgO</b>	0.01	0.15	0.03	0.03	0.00	0.00
<b>NiO</b>	0.00	0.00	0.00	0.00	0.00	0.00
<b>GT</b>	100.37	100.38	101.33	100.68	100.39	100.25
<b>Al</b>	1.297	1.267	1.276	1.294	1.292	1.286
<b>Fe</b>	0.013	0.031	0.001	0.009	0.007	0.008
<b>Ti</b>	0.001	0.000	0.000	0.000	0.000	0.000
<b>Zn</b>	0.000	0.000	0.000	0.000	0.000	0.000
<b>Si</b>	2.688	2.697	2.716	2.688	2.697	2.698
<b>K</b>	0.017	0.018	0.011	0.019	0.010	0.014
<b>Ca</b>	0.322	0.317	0.298	0.326	0.329	0.320
<b>Na</b>	0.663	0.672	0.691	0.671	0.647	0.681
<b>Cr</b>	0.000	0.000	0.000	0.000	0.002	0.000
<b>Mn</b>	0.000	0.002	0.001	0.001	0.000	0.000
<b>Mg</b>	0.001	0.010	0.002	0.002	0.000	0.000
<b>Ni</b>	0.000	0.000	0.000	0.000	0.000	0.000
Soma-Cát.	5.002	5.014	4.996	5.010	4.984	5.007
Soma-O	8.000	8.000	8.000	8.000	8.000	8.000
<b>X<sub>An</sub></b>	0.321396596	0.314871	0.29771	0.320769	0.333611	0.315558
<b>X<sub>Ab</sub></b>	0.661621647	0.667626	0.691091	0.660859	0.656057	0.670465

<b>DataSet/Point</b>	<b>38 / 1 .</b>	<b>44 / 1 .</b>	<b>45 / 1 .</b>
<b>Phase</b>	<b>Bt incl Gt</b>	<b>Bt</b>	<b>Bt</b>
<b>Na2O</b>	0.28	0.04	0.08
<b>SiO2</b>	36.15	35.04	35.04
<b>MgO</b>	9.61	7.26	7.94
<b>Al2O3</b>	13.86	13.01	12.4
<b>K2O</b>	8.9	9.38	9.09
<b>CaO</b>	0.07	0.2	0.08
<b>TiO2</b>	5.76	5.56	5.92
<b>Cr2O3</b>	0.00	0.00	0.00
<b>FeO</b>	21.02	22.24	23.1
<b>MnO</b>	0.02	0.01	0.01
<b>GT</b>	95.66	92.76	93.66
<b>Na</b>	0.043	0.006	0.013
<b>Si</b>	2.872	2.913	2.887
<b>Mg</b>	1.138	0.900	0.975
<b>Al</b>	1.298	1.275	1.204
<b>K</b>	0.902	0.995	0.955
<b>Ca</b>	0.006	0.018	0.007
<b>Ti</b>	0.344	0.348	0.367
<b>Cr</b>	0.000	0.000	0.000
<b>Fe</b>	1.397	1.546	1.592
<b>Mn</b>	0.001	0.001	0.001
Soma-Cát.	8.001	8.001	8.001
Soma-O	11.394	11.398	11.373
<b>X<sub>Fe</sub></b>	0.551015	0.632188	0.620112
<b>X<sub>Mg</sub></b>	0.448985	0.367812	0.379888

## ZIRCON SATURATION TEMPERATURE

It was recognized in the early 1980s that accessory minerals (ex. Zircon ,Apatite , Monazite etc) were the most important hosts for geochemically important trace elements such as U, Th and Ree (Fourcade and Allegre, 1981; Gromet and Silver, 1983; Harrison et al., 1986), which inspired experimental studies into their solubility in crustal melts (Harrison and Watson, 1983; Watson and Harrison, 1983; Harrison and Watson, 1984; Rapp and Watson, 1985).

Because of its near ubiquitous presence in continental rocks, the solubility of zircon in a variety of melt compositions was the first to be extensively investigated (Watson, 1979; Dickinson and Hess, 1982; Harrison and Watson, 1983; Watson and Harrison, 1983). Such experimental studies indicate that zircon solubility in crustal melts is dominantly controlled by temperature and melt composition. Zircon solubility in crustal melts is insensitive to pressure change (up to 25 Kbar) or in presence of variable water content in the melt. So, from proper knowledge of the melt composition we can identify the temperature of the zircon crystallization from the magmatic body.

Their summary model for zircon solubility was given by:

$$\ln(D_{Zr}) = 12900/T(K) - 0.85(M-1) - 3.80 \dots \dots (1)$$

where  $\ln(D_{Zr})$  is the distribution coefficient determined by ratioing the zirconium abundance [Zr] for zircon (i.e., [Zr] = 500,000 ppm) and melt (in ppm). The parameter  $M = (Na + K + 2Ca)/(Al + Si)$  is an appropriate

compositional proxy for the chemical interactions through which zircon is dissolved. The results of these experiments have been widely used to predict the occurrence of zircon in crustal magmas and to estimate the peak temperature experienced by magmatic rocks (i.e., accessory mineral thermometry).

However, it was Boehnke et al. 2007, who modified the model and came up with a different formula for calculation of the Zircon saturation temperature.

$$\ln(D_{Zr}) = (10108 \pm 32)/T(K) - (1.16 \pm 0.15)(M-1) - (1.48 \pm 0.09) \dots \dots (2)$$

The model parameters in Eq.(2) are broadly similar to those of Watson and Harrison (1983) with differences arising from the improved analytical and computational methods. Comparison of the original and new models (with a nominal 5% error in T) for a constant M of 1.4 shows generally similar temperatures, although the models diverge as M increases.

However, scarcity of appropriate minerals and low temperature re-equilibration may induce difficulties to calculate the temperature of magmas that crystallized under plutonic condition (Miller et al., 2003). Zircon and apatite are the most common accessory minerals in intermediate to felsic rocks and as their solubility depends mostly upon temperature, they can serve as geothermometers, for knowing the crystallization temperatures of the granitic magma.

Using the compositions determined from our samples, zircon-saturation temperature calculated from the equation of Watson and Harrison (1983) is  $820 \pm 26^{\circ}\text{C}$  (varies from 795 to  $865^{\circ}\text{C}$ ) for the porphyritic ferroan granitoid. From the equation of Boehnke et al. 2013, the estimated temperature is  $773 \pm 29^{\circ}\text{C}$  (739 to  $821^{\circ}\text{C}$ ).

Zircon saturation temperature can also sometimes result in anomalously high temperatures, if Zircon xenocrysts are present, which do not contribute any Zr to the melt, but can affect the Zr data in case of bulk calculation. Zircon is mostly uniform and no such xenocrysts have been observed and thus the Zircon saturation temperature can be relied upon.

# GEOCHEMISTRY

## Analytical Method

A total of nine samples were selected for major element geochemical analysis. Due to the porphyritic nature of the rock heterogeneity is quite evident. To nullify the effects of the porphyritic nature of the rock during whole rock bulk analysis rock samples were collected of quite large size compared to the porphyritic grains. Also samples are taken from comparatively unweathered and unaltered fresh rock sections. Powdering of the rock samples were done using jaw crusher and followed by Pulverizer.

Major oxide analyses were carried out in the X-ray Fluorescence laboratory of National Centre for Earth Science Studies (NCESS), India. Major element abundances were analyzed by X-ray fluorescence (XRF) on fused disks using a Bruker S4 Pioneer sequential wavelength-dispersive X-ray spectrometer. Details of the methodology used in these laboratories are discussed in Ravindra Kumar and Sreejith (2016). Standards used for the analyses are G2, GSP2, STM1, SARM1, SARM2, SY3, RGM, GA, GH, GSN, AC-E, MDOG, ISHG, VS-N, JG-1, JG-2, JG-3, JR-3 and JSY-1.

Trace element analyses were carried out by laser ablation – inductively coupled plasma – mass spectrometry (LA-ICP-MS) in Activation Laboratories, Canada, following a lithium metaborate–tetraborate fusion and dilute nitric acid digestion of a 0.1 g sample. For most of the REEs, high field strength elements (Nb, Ta, Y, Hf, Th, U) detection limit varies from 0.1 to 1 ppm whereas for Pb the limit is 5 ppm and for Rb and Sr it is 2 ppm.

## GEOCHEMISTRY

Geochemical data shows that all the samples belong to the granodiorite field in QAP diagram (ref)(fig4a). This classification is done by the CIPW Norm calculation on the basis of the whole rock bulk composition (table) and also on the basis of modal calculation. All the samples are characterized by extreme iron enrichment with  $\{FeOt/(FeOt+MgO)=0.8-1\}$  (fig4d) , having an  $SiO_2$  content of 61%-67%. The rocks are mostly calc-alkalic , metaluminous to slightly peraluminous in character with  $A/NK = 1.4-1.9$  and  $ASI = 0.9-1.1$ (fig4b and 4c)(Frost et al 2001) .

In the major oxide vs  $SiO_2$  diagrams,  $FeO_t$ ,  $TiO_2$  and  $P_2O_5$  show a general decrease, with increase in  $SiO_2$  content , whereas  $K_2O$ ,  $Al_2O_3$  and  $CaO$  do not show any discernable trends (Fig 7).  $Na_2O$  content is higher than  $K_2O$  , with average  $Na_2O / K_2O$  being around 1.4. It shows high concentrations of LILE ( like Rb, Ba etc) and HFSE ( like Zr, Nb, Ta etc)

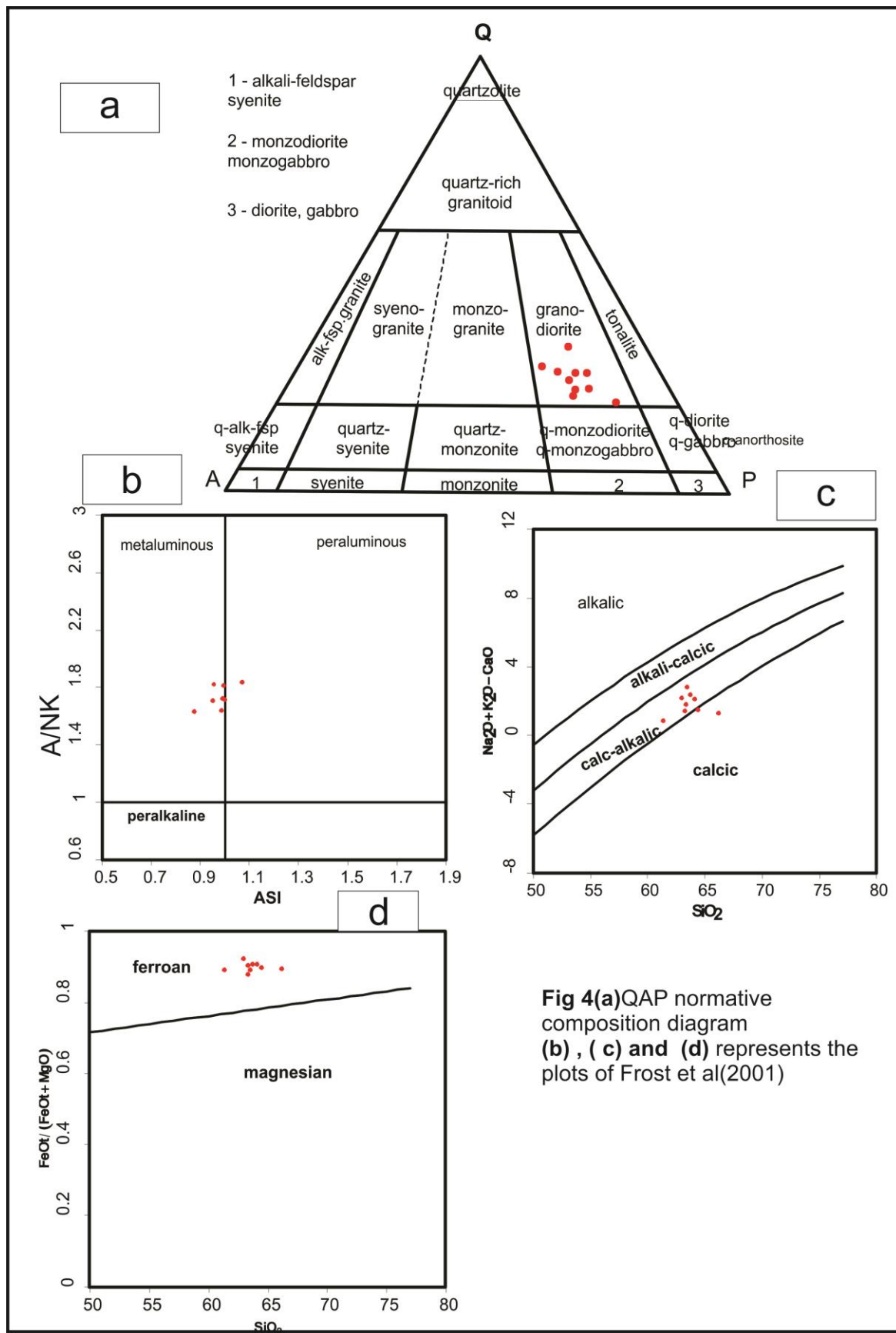
Chondrite normalized REE patterns(after McDonough and Sun, 1995) also show a slightly negative slope, showing moderate LREE enrichment and flat HREE trends, with  $(La/Lu)_N$  normalized values ranging between 2.7-6.2. Moderately negative Eu anomaly (  $Eu/Eu^*=0.55-1.04$ ) is observed as well. (Fig 5a)

Primitive mantle normalized trace element spider diagram(normalization values after McDonough and Sun, 1995), shows a monotonously decreasing abundance pattern, characterized by significant negative anomalies of Cs, Sr and Ti and relative enrichment of Rb, Ba and Ta. (FIG 5b)

Zr and  $(Zr + Hf)$  both show increasing trend with increasing  $SiO_2$  content.(fig 5c and 5d) .Rb and Ba decreases with increasing  $SiO_2$  content (fig6a

and 6b).Sr also shows a decreasing trend with decreasing SiO<sub>2</sub> (fig 6c). Other trace elements however, do not show any discernable trends.(fig 6d,6e and 6f)

Extreme Fe-enrichment, over the range of SiO<sub>2</sub> spread, classifies the rock as a “Ferroangranitoid” and high HFSE abundances( Zr, Nb, etc) couples with high Ga/Al ratio further strengthens its claims of being ” A-type Granitoid” (after Frost et al., 2001; Frost and Frost, 2011)(fig4b,4c and 4d).



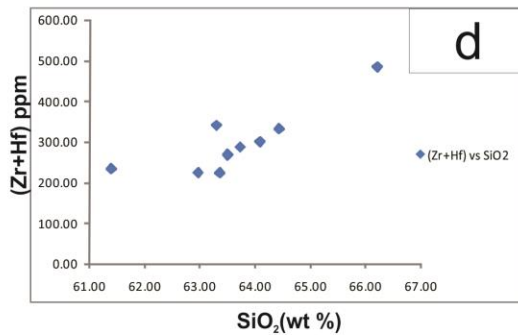
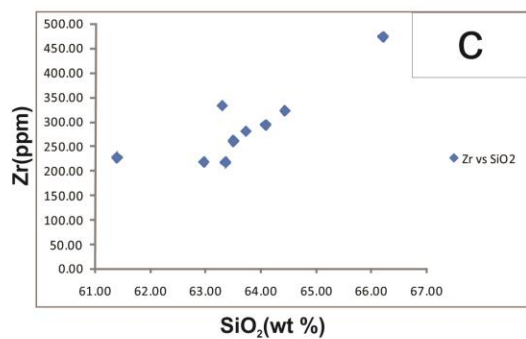
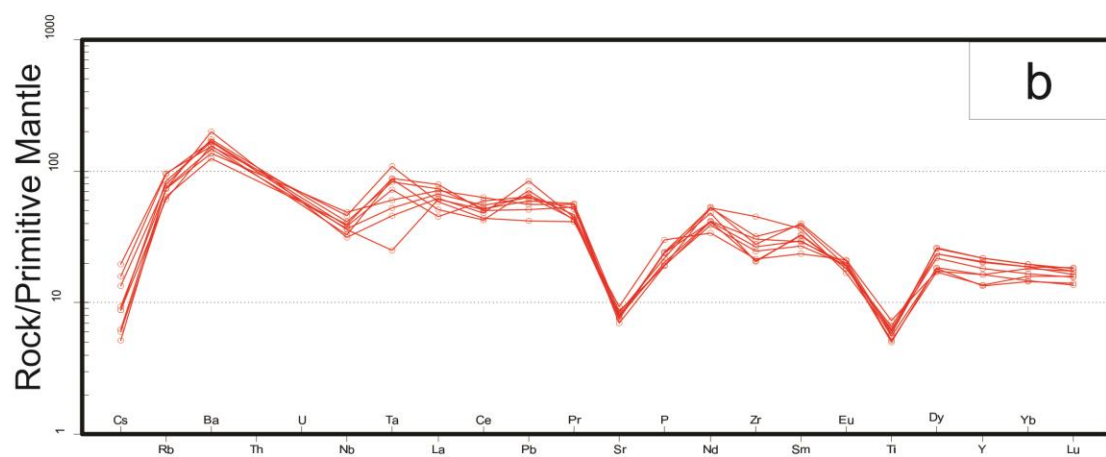
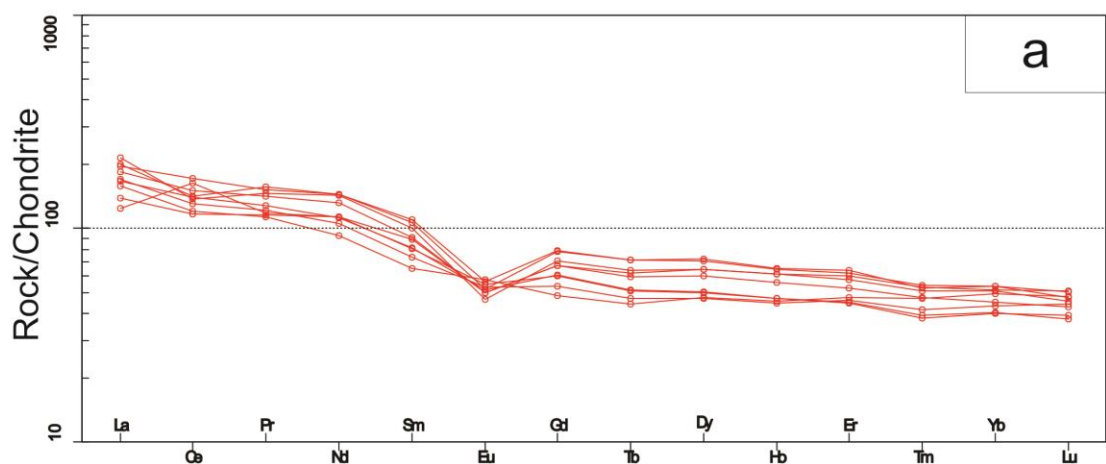


**Fig 5(a)** Chondrite normalised REE plot

**Fig 5(b)** Primitive mantle normalised trace element discrimination diagram

**Fig 5( c)** Zr vs  $\text{SiO}_2$  diagram

**Fig 5(d)** (Zr+Hf) vs  $\text{SiO}_2$

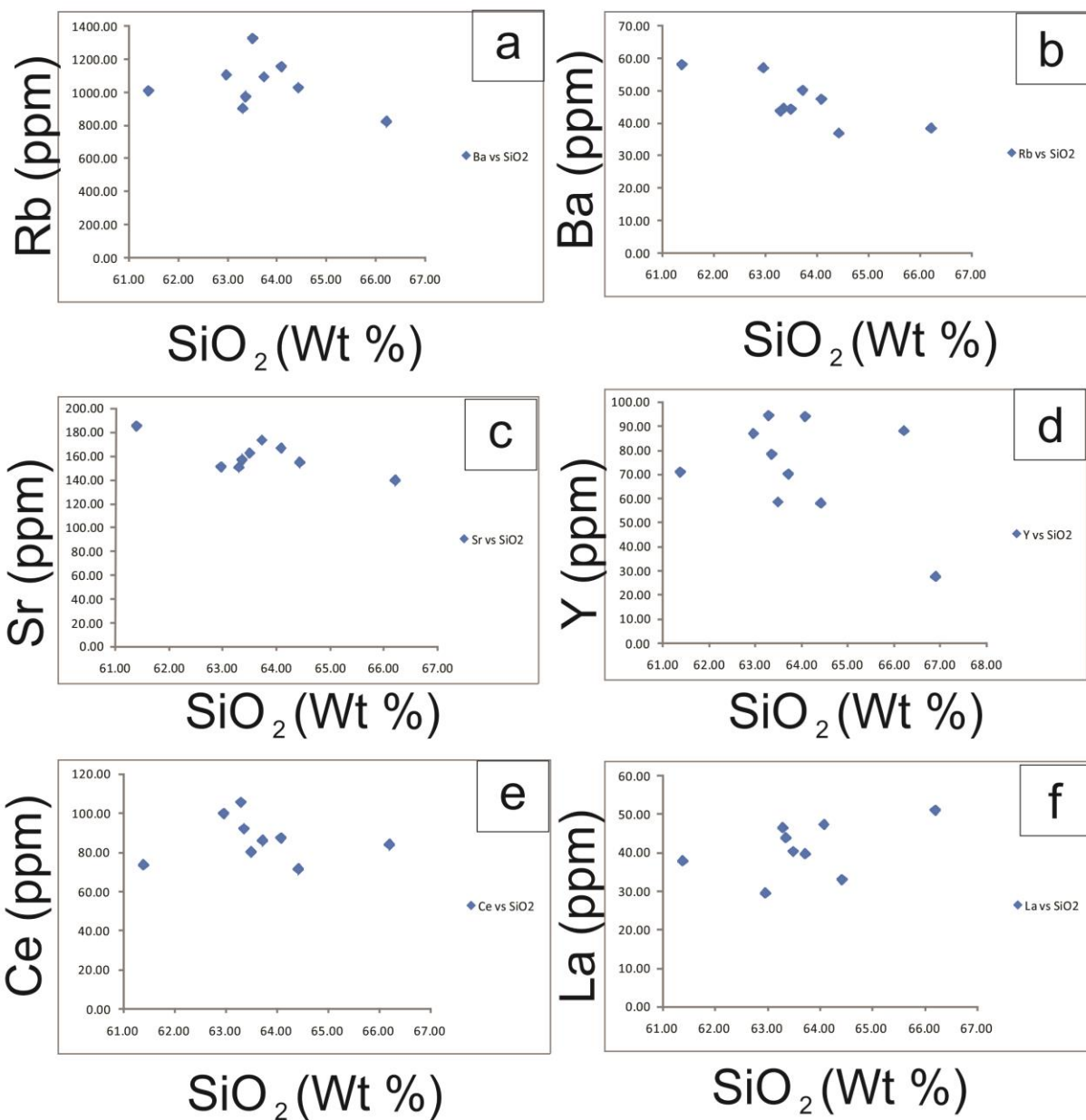


Fig 6(a)Ba vs SiO<sub>2</sub> graph  
 6(b) Rb vs SiO<sub>2</sub> graph  
 6(c) Sr vs SiO<sub>2</sub> graph  
 6(d) Y vs SiO<sub>2</sub> graph  
 6(e) Ce vs SiO<sub>2</sub> graph  
 6(f) La vs SiO<sub>2</sub> graph

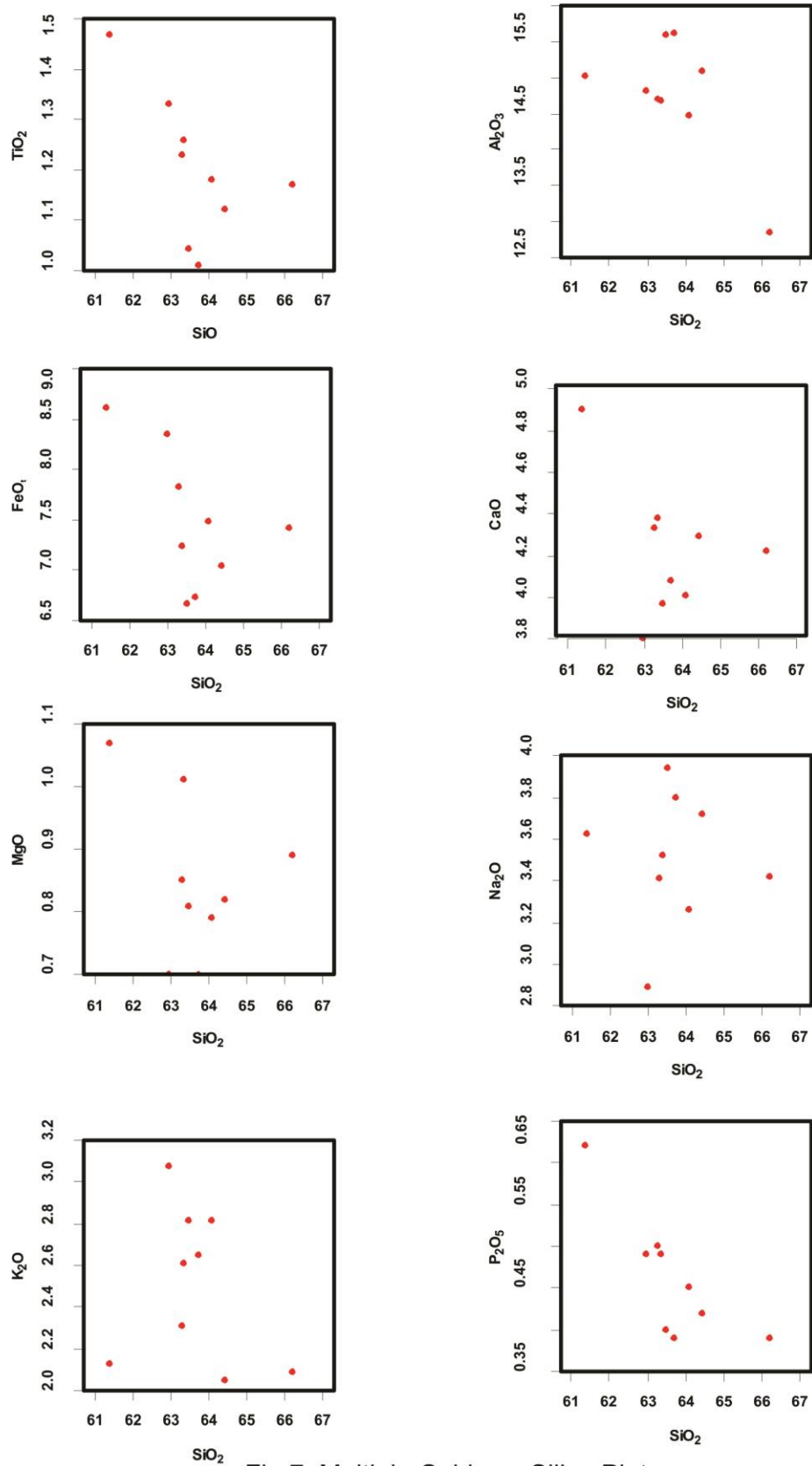


Fig 7. Multiple Oxide vs Silica Plots

**Table No 2 . Representative major oxide data from Bulk Rock Analysis of Porphyritic Granitoid.**

Sample No.	SD1	SD2	SD9A	SD11	SD12	SD14	SD15	SD16	SD17
SiO <sub>2</sub>	66.22	61.39	64.09	64.43	63.73	62.97	63.50	63.36	63.30
TiO <sub>2</sub>	1.17	1.47	1.18	1.12	1.01	1.33	1.04	1.26	1.23
Al <sub>2</sub> O <sub>3</sub>	12.83	15.02	14.48	15.08	15.63	14.82	15.60	14.68	14.71
Fe <sub>2</sub> O <sub>3</sub>	8.24	9.57	8.31	7.81	7.47	9.27	7.39	8.04	8.69
FeOT	7.42	8.61	7.48	7.03	6.72	8.34	6.65	7.24	7.82
MnO	0.13	0.17	0.15	0.15	0.14	0.17	0.14	0.15	0.16
MgO	0.89	1.07	0.79	0.82	0.70	0.70	0.81	1.01	0.85
CaO	4.22	4.90	4.01	4.29	4.08	3.80	3.97	4.38	4.33
Na <sub>2</sub> O	3.42	3.62	3.26	3.72	3.80	2.89	3.94	3.52	3.41
K <sub>2</sub> O	2.09	2.13	2.81	2.05	2.65	3.07	2.81	2.61	2.31
P <sub>2</sub> O <sub>5</sub>	0.39	0.62	0.45	0.42	0.39	0.49	0.40	0.49	0.50

**Table No 3 . Representative Trace element data from Bulk Rock Analysis of Porphyritic Granitoid.**

Sample No.	SD1	SD2	SD9A	SD11	SD12	SD14	SD15	SD16	SD17
Li	6.18	8.46	7.10	8.17	5.13	6.73	7.31	7.01	6.65
Be	2.32	3.59	2.21	2.22	2.64	2.28	1.99	2.24	2.52
Sc	17.93	22.62	20.13	17.01	17.42	21.71	17.48	18.72	22.11
V	71.56	86.68	71.82	55.54	65.69	91.98	58.49	81.09	78.03
Cr	8.21	14.35	12.06	9.38	11.53	11.66	11.09	9.92	13.27
Mn	965.65	1373.33	1118.25	998.29	1082.09	1211.14	999.23	1154.15	1253.66
Co	106.87	69.70	96.38	105.07	84.56	87.99	71.98	87.80	75.22
Ni	5.11	8.54	4.62	7.18	7.13	10.07	6.51	7.12	6.55
Cu	13.22	17.05	12.11	14.27	12.24	15.22	14.65	15.05	15.44
Zn	154.00	204.02	173.94	150.66	153.51	169.60	150.21	164.75	185.53
Ga	23.63	25.17	25.25	23.16	26.62	25.88	22.68	24.75	26.28
Ge	5.67	5.30	5.79	4.65	4.90	5.45	4.53	5.13	5.85
Se	6.44	3.54	7.04	4.25	4.64	5.39	3.82	5.62	6.01
Rb	38.24	58.09	47.38	36.67	50.07	57.02	44.28	44.44	43.71
Sr	139.50	184.79	166.30	154.44	173.02	150.73	162.17	156.66	150.24
Y	87.76	70.79	93.68	57.76	69.85	86.63	58.27	78.17	94.09
Zr	472.67	226.85	293.08	322.03	279.96	217.65	260.47	216.89	332.46
Nb	26.09	30.36	26.94	21.71	23.56	25.03	20.59	24.11	31.89
Mo	1.28	2.01	0.99	1.73	0.98	1.26	1.59	1.62	1.40
Cd	0.61	0.46	0.45	0.51	0.43	0.37	0.43	0.35	0.53
Sn	1.88	1.19	0.88	1.02	1.09	1.27	0.90	0.97	1.43
Sb	0.02	0.03	0.01	0.04	0.20	0.01	bdl	0.00	0.17
Te	0.06	0.06	0.15	0.05	0.04	0.04	0.03	0.03	0.04
Cs	0.13	0.41	0.28	0.18	0.18	0.33	0.13	0.11	0.20
Ba	824.20	1010.13	1156.60	1029.28	1093.11	1106.91	1326.60	974.83	903.38
La	50.94	37.71	47.20	32.87	39.54	29.32	40.25	43.73	46.35

Sample No.	SD1	SD2	SD9A	SD11	SD12	SD14	SD15	SD16	SD17
<b>Ce</b>	83.89	73.56	87.30	71.40	85.97	99.79	80.18	92.07	105.53
<b>Pr</b>	13.52	10.52	14.49	10.78	11.83	11.02	11.31	13.20	14.14
<b>Nd</b>	65.41	42.53	66.27	51.95	51.24	51.88	48.19	60.19	66.04
<b>Sm</b>	14.84	9.59	16.31	11.86	12.06	13.15	10.87	13.40	15.80
<b>Eu</b>	2.61	3.25	3.19	3.08	2.91	2.82	2.99	2.81	2.93
<b>Gd</b>	14.03	9.67	15.75	11.91	12.01	13.35	10.68	13.41	15.57
<b>Tb</b>	2.31	1.60	2.57	1.84	1.85	2.23	1.70	2.14	2.57
<b>Dy</b>	15.77	11.75	17.74	12.29	12.45	15.79	11.57	14.71	17.39
<b>Ho</b>	3.35	2.50	3.55	2.56	2.56	3.34	2.44	3.04	3.53
<b>Er</b>	9.62	7.64	10.22	7.16	7.26	9.23	7.40	8.39	9.88
<b>Tm</b>	1.32	1.16	1.30	0.94	0.97	1.26	1.03	1.18	1.33
<b>Yb</b>	8.31	7.97	8.69	6.43	6.51	8.23	6.97	7.32	8.64
<b>Lu</b>	1.26	1.18	1.17	0.96	0.92	1.12	1.09	1.06	1.24
<b>Hf</b>	11.29	5.47	7.00	8.71	6.75	5.56	6.98	5.40	7.81
<b>Ta</b>	3.24	4.05	3.08	3.21	0.92	2.68	1.71	1.95	2.22
<b>Tl</b>	0.11	0.17	0.13	0.12	0.14	0.15	0.15	0.13	0.11
<b>Pb</b>	7.67	6.29	8.85	10.61	9.87	9.67	12.56	9.43	8.38
<b>Bi</b>	0.03	0.06	0.01	0.01	0.01	0.02	0.01	0.01	0.02
<b>Eu/Eu*</b>	0.551958	1.029132	0.606846	0.79023	0.737895	0.64808	0.844505	0.639715	0.568735
<b>(La/Lu)<sub>N</sub></b>	4.194632	3.318238	4.172018	3.548321	4.439713	2.719643	3.849297	4.284237	3.869822
<b>(Y/Nb)<sub>N</sub></b>	0.514666	0.356786	0.53218	0.830726	0.407201	0.453725	0.529746	0.432994	0.496129
<b>(Ta/Nb)<sub>N</sub></b>	2.211438	2.373696	2.034708	2.62867	0.697447	1.907858	1.475655	1.437441	1.235649
<b>T(°C) Watson</b>	864.0347	794.1129	829.7912	840.2135	827.881	809.1166	819.0092	795.6841	839.9819
<b>T( °C)Boehnke</b>	821.2572	739.41	786.1188	799.0488	784.9004	764.7544	773.5531	743.5474	797.3552

# DISCUSSION

## ❖ MAJOR AND TRACE ELEMENT BEHAVIOUR:

The coherent trends produced in the Harker diagrams, can result from any of the four possibilities (reviewed in Wilson, 1993)

- I) variable degree of crustal assimilation with ascending melt
- ii) magma mixing/ mingling
- iii) fractionation of different phases
- Iv) metamorphic segregation

Magma mixing or mingling dominantly requires a mafic magma that frequently produce local hybrid zones and mafic enclaves, presumed to be coherent with the granite. But in our field area, though there were mafic enclaves, field relations clearly show that their solidification predates the granitic intrusion. Absence of hybrid zones and moreover the restricted range of elements, especially  $\text{SiO}_2$ , clearly depicts the limited magma mixing/ mingling.(Pitcher, 1997).

Decreasing  $\text{FeO}_t$  content with increasing  $\text{SiO}_2$  suggest a progressive fractionation of ferromagnesian phases (i.e. mainly pyroxenes) whereas negative correlation of  $\text{P}_2\text{O}_5$  with  $\text{SiO}_2$  can be attributed to crystallisation of apatite, along with some other silicate phases. Ilmenite fractionation may explain the decrease in  $\text{TiO}_2$  and  $\text{FeO}_t$  with  $\text{SiO}_2$ . It has been observed that HFSE and REE budget of the rocks are largely controlled by accessory phases and is more pronounced in cases of peraluminous rocks, as compared to metaluminous granites. However, Ba, Sr and Rb content are mostly determined by the crystallisation of feldspar phases and biotite content.

The relative changes, in concentration of Ba and Sr clearly depicts that both Kfs and Plagioclase had crystallised simultaneously. Let us assume that the max point, in the graph corresponds to the initial Ba and Sr ratios in the melt. Our data trend, are not parallel to any of the trends of either only Kfs or only Plag crystallisation and so, it can be inferred that both were crystallising simultaneously, though it can't be quantified as we lack knowledge of the initial Ba/Sr ratios and we also do not know in what proportion they crystallised, but we can say qualitatively that both were crystallising simultaneously.

❖ **Nature of magma source :**

The source of the ferroan granitoids has been a topic of huge debate, as it involves a wide variety of rock types. Contrasting chemical nature of these different sources, coupled with the involved petrogenetic processes, dictates the relative involvement of mantle or crust during ferroan A-type granitoid generation (reviewed in Bonin, 2007; Frost and Frost, 2011; Martin, 2006). Among most of the geochemical parameters, few of the trace element ratios can indicate the relative involvement of the crust or mantle, in the petrogenesis of the ferroan granitoid (Eby, 1992, 1990; Moreno et al., 2016, 2014; Pearce, 1996; Pearce et al., 1984; Whalen et al., 1987). The scheme of classification, as proposed by Eby (1990, 1992), says that in absence of any post magmatic complexities like crustal assimilation or extreme fractionation of any accessory phases, which act as a reservoir for HFSE's, Y/Nb ratio can be used as a proxy for the nature of the source. High Y/Nb ratios (2.33-5.42), along with high Ce and high Ga values, as proposed by Eby (1992), suggests that the porphyritic granite belongs to A<sub>2</sub> granites.

In our samples, high HFSE contents {  $Ta_{(N)} = (36.94-162.03$  ppm) and  $Nb_{(N)} = (48.79-71.69$  ppm)} indicates a certain involvement of mantle material with the dominant continental crust, during petrogenesis of the porphyritic ferroan A type granitoid.

❖ **ORIGIN OF MELT :**

It has been previously established by experimental studies that metaluminous to peraluminous granites, like the porphyritic granite, can be produced by low pressure (4-8 K Bar) dehydration melting of both biotite and amphibole (Clemens and Vielzeuf, 1987; Clemens and Wall 1981; Rushmer, 1991; Watkins et al., 2007)

- i) Biotite + Quartz + Plagioclase = Orthopyroxene ± Clinopyroxene ± Garnet + K-Feldspar + melt
- ii) Amphibole + Quartz = Orthopyroxene + Clinopyroxene ± Garnet + Plagioclase + melt

Biotite breakdown at lower pressure, increases the  $K_2O$  content in the melt, whereas amphibole breakdown produces a more sodic melt, mostly tonalitic to trondhjemitic in composition. (Patiño Douce and Beard, 1995; Watkins et al., 2007).

In our samples, the  $Na_2O/K_2O$  ratio is round 1.4 i.e. >1, which indicates the involvement of amphibole in the melting process. However, high Ga/Al ratio, (fig 8) along with higher Rb content, indicates towards the involvement of biotite breakdown in the source. So, it cannot be conclusively determined without further study, whether biotite was dominant or amphibole, but that both were present at the source, during the time of melting.

Although post-emplacement fractionation can influence the REE and trace element contents, overall flat REE pattern with moderate LREE/HREE ratio, negative Eu anomaly and Sr depletion suggests the predominance of Plagioclase over Garnet, suggesting low pressure melting.

Production of such melt fractions requires high heat supply which requires the involvement of the mantle or mantle-derived magmas as a source for this heat because heat produced by the decay of radioactive elements (e.g., K, U and Th) within a thickened crust would be insufficient to produce such high heat flow (Clemens, 1984; Sylvester, 1989). Moreover, the porphyritic granite is devoid of U or Th and thus the theory of radioactive heating doesn't hold any wind.

The shallow depth and moderately high temperature of melting of the porphyritic granite, are therefore indicative of anatexis by regional crustal thinning associated with underplating of mafic magmas and/or mantle upwelling, rather than being the result of an over-thickened continental crust .

#### ❖ **TECTONIC AFFINITY:**

The characterization of these ferroan (A-type) granitoids, in terms of their tectonic affinity, has remained a topic of discussion.

Unequivocal acceptance ,by geoscientists, of these granites belonging to 'anorogenic' settings(Loiselle and Wones,1979).has been challenged at various points, as granites formed through post-orogenic and late-orogenic processes also have similar geochemical characteristics (Eby, 1992, 1990; Whalen et al., 1987)

It has been observed that, A-type granitoids are associated with extensional (non-compressional)settings either in continental-rift zones, at the end of the orogenic cycle or in ocean rift settings (Bonin, 2007; Clemens et al.,

1986; Dall'Agnol et al., 2012,2005; Eby, 1992; Oliveira et al., 2009; Martin, 2006; Medlin et al.,2014; Montero et al., 2009; Moreno et al., 2016, 2014, 2017; Nironenet al., 2000; Rogers and Greenberg, 1990; Sylvester, 1989; Whalenet al., 1987).

As obtained from the geochemical data, it can be said that the source of these granites are dominated by continental crust. Geochemical discrimination parameters, like Y/Nb ratio,used by Eby(1992) can be similar in cases of both, late or post-orogenic melting of continental crust, as well as the melting of the same crust, in a completely unrelated anorogenic process. The geochemical discrimination parameters, like Y/Nb ratios, can be better used to understand the character of the source, rather than the tectonic environment. In the plots of Eby et al (1990,1992) , the rock is characterized as an A<sub>2</sub> –type granitoid, which indicates a post orogenic setup.(Fig 9)

The plots of Pearce et al.(1984) , uses Rb, Y, Nb, Ta and Yb, for characterization of the tectonic environment of the emplaced granite. The reason for using these elements are justified:-

- i) Y and Yb are generally more abundant in normal ocean ridges and Within Plate Granites(WPG), as compared to Volcanic Arc Granites (VAG)
- ii) Rb forms an almost perfect discriminator, between Ocean Ridge and Within Plate Granites(higher Rb content).
- iii) Nb and Ta are generally more enriched in Within Plate Granite(WPG) than in any other type of granites, with the exception of granites intruded in within plate granites, in areas of attenuated continental lithosphere, which causes overlapping with other granite types.

The geochemical data of the porphyritic granite, plots all the samples of the porphyritic granitoid, inside the “Within Plate Granite(WPG)” field ,in the plots of Pearce et al.(1984)(Fig 10)

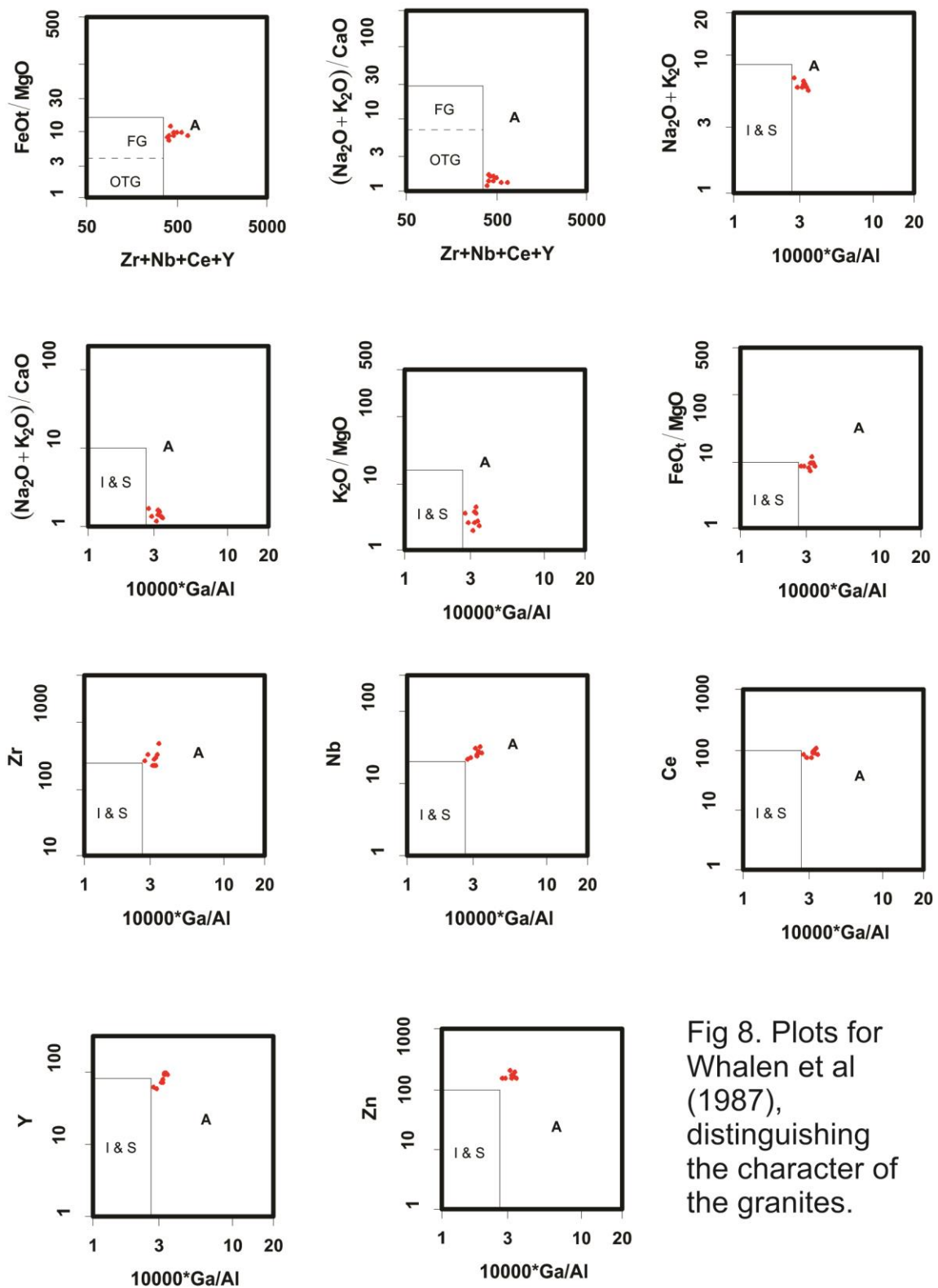
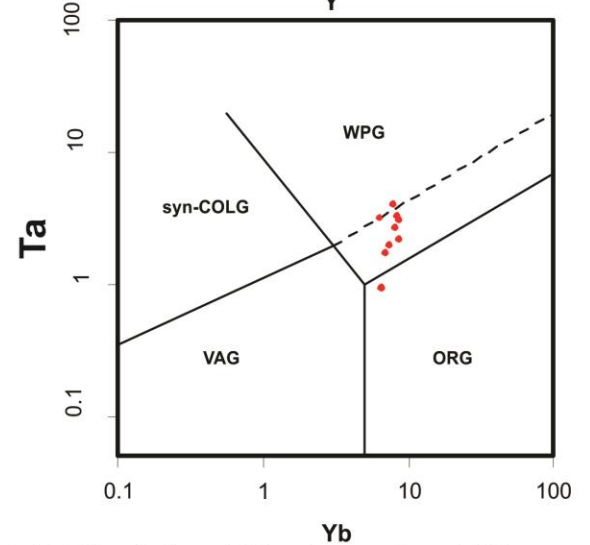
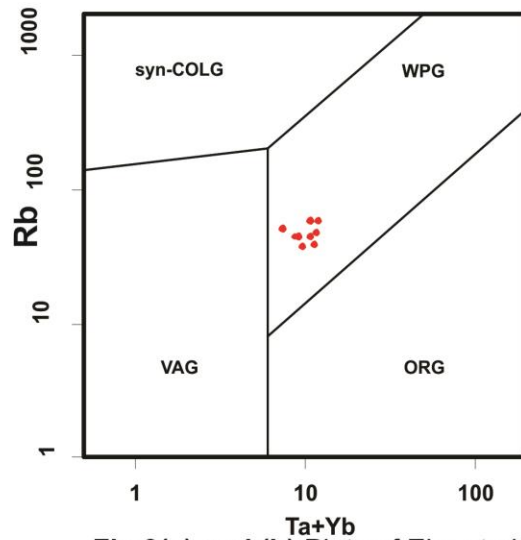
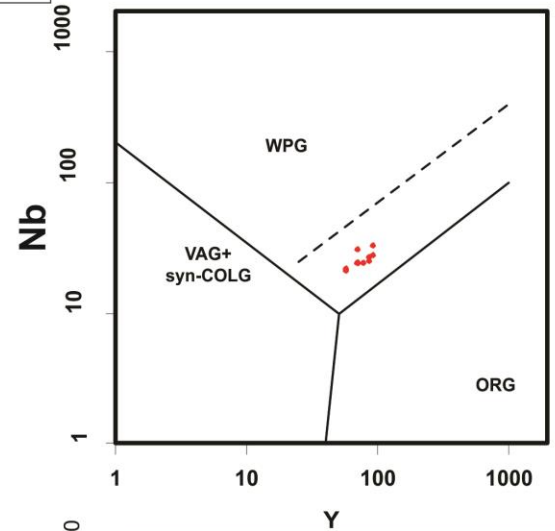
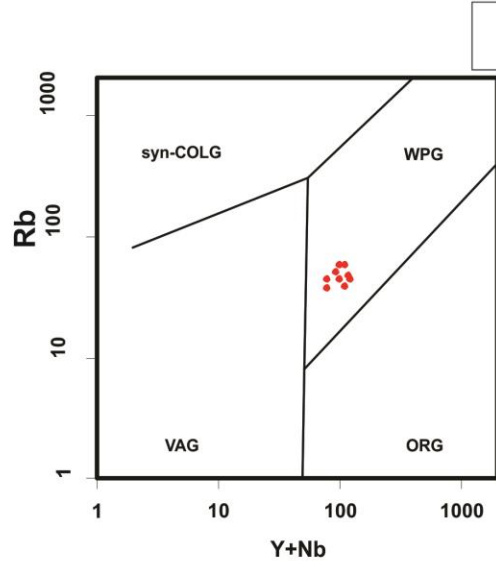
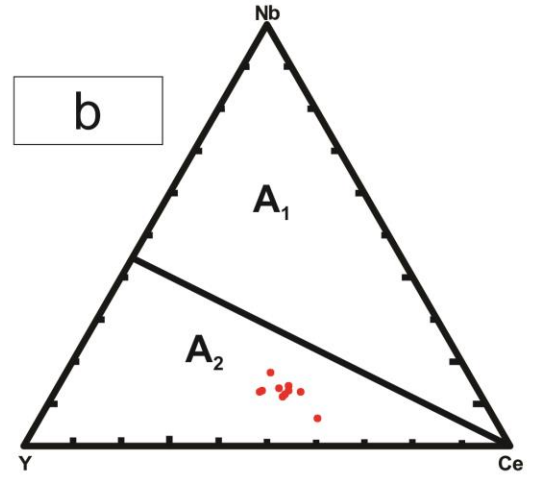
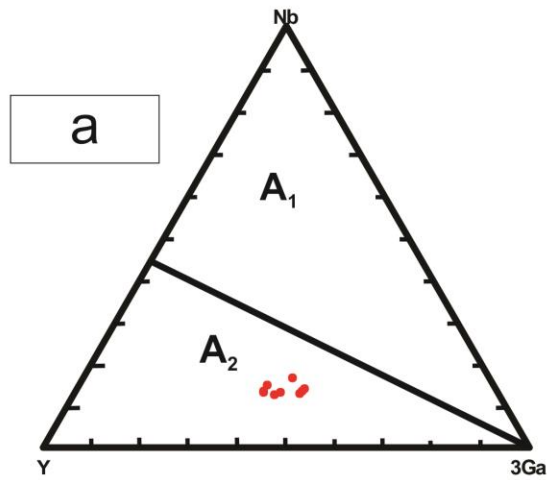


Fig 8. Plots for Whalen et al (1987), distinguishing the character of the granites.



**Fig 9(a) and (b)** Plots of Eby et al(1990,1992) , distinguishing A type Granitoids  
**Fig 9( c)** Plots of Pearce et al(1984) , distinguishing the tectonic affinity of the granitoid.

# **MINERAL ABBREVIATIONS**

Grt: Garnet

Cpx: Clinopyroxene

Amp: Amphibole

Pl: Plagioclase

Qtz: Quartz

Ilm: Ilmenite

Bt: Biotite

Kfs: K-feldspar

Mag:Magnetite

Opx:Orthopyroxene

# REFERENCES

---

- Eby, G.N., 1992. Chemical subdivision of the A-type granitoids: petrogenetic and tectonic implications. *Geology*, 20(7), pp.641-644.
- Eby, G.N., 1990. The A-type granitoids: a review of their occurrence and chemical characteristics and speculations on their petrogenesis. *Lithos*, 26(1-2), pp.115-134.
- Frost, B.R., Barnes, C.G., Collins, W.J., Arculus, R.J., Ellis, D.J. and Frost, C.D., 2001. A geochemical classification for granitic rocks. *Journal of petrology*, 42(11), pp.2033-2048.
- Frost, C.D. and Frost, B.R., 2010. On ferroan (A-type) granitoids: their compositional variability and modes of origin. *Journal of petrology*, 52(1), pp.39-53.
- Whalen, J.B., Currie, K.L. and Chappell, B.W., 1987. A-type granites: geochemical characteristics, discrimination and petrogenesis. *Contributions to mineralogy and petrology*, 95(4), pp.407-419.
- Pearce, J.A., Harris, N.B. and Tindle, A.G., 1984. Trace element discrimination diagrams for the tectonic interpretation of granitic rocks. *Journal of petrology*, 25(4), pp.956-983.
- Mukherjee, S., Dey, A., Ibanez-Mejia, M., Sanyal, S. and Sengupta, P., 2018. Geochemistry, U-Pb geochronology and Lu-Hf isotope systematics of a suite of ferroan (A-type) granitoids from the CGGC: Evidence for Mesoproterozoic crustal extension in the east Indian shield. *Precambrian Research*, 305, pp.40-63.
- Boehnke, P., Watson, E.B., Trail, D., Harrison, T.M. and Schmitt, A.K., 2013. Zircon saturation re-revisited. *Chemical Geology*, 351, pp.324-334.

Watson, E.B. and Harrison, T.M., 1983. Zircon saturation revisited: temperature and composition effects in a variety of crustal magma types. *Earth and Planetary Science Letters*, 64(2), pp.295-304.

Ray, B., Bishui, P.K., Mukhopadhyay, K. and Ray, J.N., 1994. Rb-Sr geochronology of the high-grade rocks from Purulia, West Bengal and Jamua-Dumka sector, Bihar. *Indian Minerals*, 48(1-2), pp.45-60.

Miller, C.F., McDowell, S.M. and Mapes, R.W., 2003. Hot and cold granites? Implications of zircon saturation temperatures and preservation of inheritance. *Geology*, 31(6), pp.529-532.

Pitcher, W.S., 1997. *The nature and origin of granite*. Springer Science & Business Media.

Bonin, B., 2007. A-type granites and related rocks: evolution of a concept, problems and prospects. *Lithos*, 97(1-2), pp.1-29.

Clemens, J.D. and Vielzeuf, D., 1987. Constraints on melting and magma production in the crust. *Earth and Planetary Science Letters*, 86(2-4), pp.287-306.

Clemens, J.D., Holloway, J.R. and White, A.J.R., 1986. Origin of an A-type granite; experimental constraints. *American Mineralogist*, 71(3-4), pp.317-324.

Rushmer, T., 1991. Partial melting of two amphibolites: contrasting experimental results under fluid-absent conditions. *Contributions to Mineralogy and Petrology*, 107(1), pp.41-59.

Du, L., Yang, C., Wyman, D.A., Nutman, A.P., Lu, Z., Song, H., Xie, H., Wan, Y., Zhao, L., Geng, Y. and Ren, L., 2016. 2090–2070 Ma A-type granitoids in Zanzhuang Complex: further evidence on a Paleoproterozoic rift-related tectonic regime in the Trans-North China Orogen. *Lithos*, 254, pp.18-35.

Sylvester, P.J., 1989. Post-collisional alkaline granites. *The Journal of Geology*, 97(3), pp.261-280.

Dall'Agnol, C.M., Magalhães, A.M.M.D., Mano, G.C.D.M., Olschowsky, A. and Silva, F.P.D., 2012. A noção de tectonofocos. *Revista gaúcha de enfermagem*. Porto Alegre. Vol. 33 n. 1 (mar. 2012), p. 186-190.

Rogers, J.J. and Greenberg, J.K., 1990. Late-orogenic, post-orogenic, and anorogenic granites: distinction by major-element and trace-element chemistry and possible origins. *The Journal of Geology*, 98(3), pp.291-309.

# **ACKNOWLEDGEMENT**

I would like to render my sincere gratitude to my professor and guide, Prof Sanjay Sanyal for his astute guidance and encouragement , throughout the period of the dissertation work. I would also like to thank, Dr.Shubham Mukherjee, Somdipta Chatterjee, Enakshi Das Dr. Shreya Karmakar, Dr.Anindita Dey, Satabdi Das ,Arimita Chakraborty and Sirina Roy Chowdhury for their relentless help and guidance in making this dissertation work a success.Finally, I would like to thank my labmate, Subho Mukherjee for his constant support.